The Retrieval of Vertical Air Velocity from High-Resolution Coherent Radar Measurements in Zenith Direction

A.M.Sabade

Delft University of Technology

TU Delft

The Retrieval of Vertical Air Velocity from High-Resolution Coherent Radar Measurements in Zenith Direction

by

A.M.Sabade

to obtain the degree of Master of Science
in Electrical Engineering
at the Delft University of Technology,
to be defended publicly on Thursday September 14, 2023.

Student number: 5564476
Thesis committee: Prof. DSc. A. Yarovoy, MS3, EEMCS, TU Delft
Dr. O. A. Krasnov, MS3, EEMCS, TU Delft
Dr. M. A. Schleiss, GRS Department, CEG, TU Delft

Cover: 'Sky During Daytime' Photo by Kenrick Mills on Unsplash

An electronic version of this thesis is available at http://repository.tudelft.nl/.

TU Delft

Acknowledgements

I would like to extend my heartfelt gratitude to everyone who has been instrumental in helping me complete my thesis. Your support, guidance, and encouragement have meant the world to me. I want to express my deep gratitude to my supervisor, Dr. Oleg Krasnov. Your guidance and insights throughout my research were truly invaluable. Your unwavering support, remarkable patience, and commitment to my academic growth were truly exceptional, and I am profoundly grateful for your contributions to my journey. I want to thank Prof. DSc. Alexander Yarovoy, the chair of our research group, for giving me the opportunity to be a part of this fantastic research community. To my friends and colleagues at the MS3 research group, your support and friendship has made this journey enjoyable and fulfilling. Our shared experiences have enriched me in countless ways.

Lastly, to my parents and my girlfriend, your unwavering belief in me and your constant encouragement have been my rock and have given me the strength to overcome challenges that come my way. Thank you for standing by me. To all of you, your contributions have been immeasurable. Your belief in me has been my inspiration, and I look forward to carrying the knowledge and experiences gained during this thesis into the next phase of my academic and professional life. Thank you for being an essential part of my journey.

A.M.Sabade

Delft, September 2023

Abstract

The use of radars for remote sensing in atmospheric sciences has become increasingly popular over the past few decades. Weather radars play a crucial role in measuring, interpreting, and monitoring various atmospheric phenomena. However, accurate retrieval of vertical air velocities remains a challenging problem owing to certain deficiencies in radar data and errors in deriving numerous parameters of precipitation. This research aims to develop data processing and air motion retrieval algorithms that can improve the accuracy of this task. The project proposes a robust data processing pipeline to enhance data reliability. It also carries out the classification of rainfall types and hydrometeor classes in the different regions of atmosphere for more accurate parameter retrieval. In this project a criteria for the quality of air-motion retrievals has been developed. The performance of the retrieval algorithms achieved by using exponential drop size distribution (DSD) for fall velocity calculations has been evaluated based on the proposed criteria. This research also aims to utilize data spanning six months for performance analysis of air velocity retrieval algorithms under various weather conditions over extensive periods of time.

Contents

List of Figures

List of Tables

Abbreviations

Abbreviations

Abbreviation	Definition
DSD	Drop Size Distribution
FFT	Fast Fourier Transform
FMCW	Frequency Modulated Continuous Wave
NETCDF	Network Common Data Form
PARSAX	Polarimetric Agile Radar in S- and X-band
PPI	Plan Position Indicator
PRF	Pulse Repetition Frequency
PRI	Pulse Repetition Interval
RADAR	Radio Detection and Ranging
RHI	Range Height Indicator

Symbols

Symbol	Definition	Unit
V	Doppler Velocity	[m/s]
Z	Reflectivity	dBZ
σ	Doppler Spectrum Width	[m/s]

1

Introduction

This chapter gives a brief introduction to weather radars and their numerous applications and describes the motivation behind retrieving and analysing vertical air velocities from radar measurements. Section 1.2 elaborates on the challenges and limitations of radars to retrieve air motion and consequently presents the research objectives. The novelties introduced in this thesis to bridge the gaps are discussed in section 1.3. Lastly, section 1.4 presents the structure of the thesis.

1.1. Introduction and Motivation for Research

After the invention of radar (**RA**dio **D**etection and **R**anging) over a century ago, the idea of weather radars took shape around the middle of the twentieth century when military radar operators noticed extensive echoes from the various atmospheric processes. Following this, a comprehensive study of these phenomena led to the development of weather radars that could be used to detect and measure precipitation and other meteorological phenomena in the atmosphere [1]. Weather radars work by transmitting electromagnetic waves, which interact with precipitation particles in the atmosphere and are scattered back to the radar receiver. The radar system then analyzes the received signals to determine the location, intensity, movement of precipitation, and several other features of the atmosphere. Over the course of time, weather radars have seen significant improvements in performance due to the continuous development of hardware and software capabilities of radar systems. Some of these are the introduction of the Doppler radar, dual-polarization radar, powerful digital signal processing techniques and high-performance computer technology. As a result, the capabilities of these radar systems have evolved from being able to detect just the presence and intensity of precipitation to measuring and analyzing the velocities, shapes, sizes, and types of precipitation particles. When compared to traditional rain gauge networks, modern-day weather radar offers more detailed and higher quality observations of precipitation systems owing to high spatial and temporal resolutions [2].

Weather radar systems are used in a variety of applications, including meteorology, aviation, transportation, and military operations. In meteorology, they are used primarily to monitor and forecast weather phenomena (such as precipitation and air motion) and to track their patterns. By utilizing radar data, the movement of storms can be tracked, and the onset and severity of weather events such as thunderstorms can be predicted. Several climate studies and models have already used radar data for various purposes [3].

An important aspect of weather radars is the retrieval of vertical air velocities from the measured data. This is a crucial application as knowledge of these velocities can be utilized for weather forecasting and generating climate models. It also provides real-time information about the location, presence, and intensity of updrafts and downdrafts, which are used to develop flight plans, make route adjustments, and issue alerts to pilots, making it critical to aviation safety. It also plays a major role in defence and space applications as precipitation intensity and wind speeds, affect mission planning and execution.

Despite the developments in radar technology, accurate retrieval of air velocities remains a challenging problem due to a number of reasons including the need for reliable radar measurements, the effects of variations in the vertical profile of the atmosphere and different types of rain, and inaccuracies that may be introduced in deriving various parameters of precipitation [2]. These challenges are discussed in detail in section 1.2.

1.2. Problem Formulation and Research Objectives

1.2.1. Problem Formulation

The challenges and limitations of measuring vertical air velocities a presented in this section. Microwave radars are unable to measure the vertical air velocities directly. To obtain vertical air velocities, the mean Doppler velocity, which represents the motion of the raindrops in the radar beam, must be measured. The measured mean Doppler velocity is a result of contributions by both the vertical air velocities and the terminal fall velocities of raindrops or any other hydrometeors. It is possible to estimate the terminal velocities by utilizing one of several relationships between drop size and fall velocity. These relationships will be discussed in detail in chapter 5. The estimated vertical air velocities are represented by the component that is obtained by subtracting the estimated terminal fall velocities from the mean Doppler velocity. This relation can be seen in equation 1.1.

$$V_{air} = V_{Doppler} - V_{Terminal}(DSD) \tag{1.1}$$

As introduced in section 1.1, accurate retrieval of vertical air velocities remains a challenging problem. This is mainly a result of various uncertainties that may be introduced due to a number of factors [2]. Some of these are listed below.

One of the most crucial requirements for accurate retrievals is reliable and high-quality radar data. This is important as radar data with deficiencies can cause errors in the derivation of various parameters and consequently the air motion. An aspect of this is correct radar calibration. Weather radar

estimates of precipitation and associated parameters depend on stable hardware components (such as the transmitter and receiver) with precise calibration. Estimates may contain significant errors due to radar calibration bias [4]. Another factor is the presence of echoes from non-meteorological targets. Measurements taken in the zenith direction may contain echoes from biological targets (like birds and insects), clear sky reflections, and miscellaneous clutter. It is important to remove these echoes to enhance the air velocity estimates.

The second factor is the variations in the vertical reflectivity profiles (VRP). The VPR exhibits significant variation due to precipitation growth, evaporation, melting of ice particles and snowflakes, and wind effects. These fluctuations show that there are significant discrepancies between radar precipitation estimates at different altitudes and precipitation that actually falls on the ground. A technique that may be employed to address this is correction based on seasons or rain types [2].

These variabilities and discrepancies in the estimates are further reflected in the drop size distribution and rainfall rate estimates. During the conversion of radar reflectivity into an estimate of rain rate at ground level, more errors and uncertainties could be added. This leads to errors in the estimation of the drop size parameters and consequently the fall velocities [5]. Therefore, there is a need to develop signal and data processing algorithms and retrieval techniques that can improve the accuracy of this task.

1.2.2. Research Objectives

Based on the formulated problem statement and the identified gaps in the reviewed literature, the following research objectives have been defined.

- Development of algorithm(s) for the retrieval of vertical air velocity.
- Deriving parameters of the drop size distribution from radar measurements.
- Classification of precipitation types and classes of hydrometoers.
- Development of retrieval quality criteria and analysis of the accuracy of the algorithm(s) based on these criteria.
- Development of an algorithm for optimal data processing, and “Big data”-based statistical analysis of retrieval techniques for validating the performance and uncertainty estimation.

1.3. Research Gaps and Novelties

Based on the reviewed literature that is described in each of the respective chapters, a number of gaps were identified in the literature. These gaps are as follows. The first is the need of multi-parameter DSD for velocity retrievals under different rainfall types and the study of the impact of various DSD parameters on the velocity retrievals. The next is the absence of large-scale analysis of vertical air velocity retrieval algorithms and the results of these algorithms with massive amounts of data.

In order to bridge these gaps, our research within this project achieved a few new results. A novel algorithm for the classification of rainfall types and regions of the vertical profiles has been developed and applied to the data in order to improve the analysis of the influence of the hydrometeor types

on the retrieval algorithms' applicability and performance. Another aspect of this project is to utilize massive data for statistical and performance analysis of velocity retrieval algorithms under various weather conditions over large periods of time. Lastly, statistics-based criteria for the quality of the air-motion retrievals are developed which coupled with the large-scale data analysis is used to quantify the performance of the aforementioned retrieval algorithms.

1.4. Thesis Structure

The thesis is structured as follows. Chapter 2 provides a brief background on the topics of radars, atmospheric remote sensing, and various precipitation types. Chapter 3 details the data processing pipeline and presents the results pertaining to data quality and reliability. Chapter 4 discusses the classification scheme implemented in this project to classify different types of rain and the classes in the vertical profile of the atmosphere. Chapter 5 presents the vertical air velocity retrieval algorithm developed for this project. Lastly, chapter 6 presents the conclusions.

2

Radar and Atmospheric Sensing Background

2.1. Radar Fundamentals

Radar is a technology that uses radiated electromagnetic energy to measure the range, velocity, and other characteristics of objects of interest. It operates on the principle of transmitting electromagnetic waves and then detecting the echoes or reflections of those waves when they bounce off objects in the environment. Broadly radars can be of two types, pulsed radars that emit short pulses and receive echo signals during the silent windows, or continuous wave radars that transmit signals continuously [6]. An overview of the Frequency Modulated Continuous Wave (FMCW) radar which is a type of continuous wave radar is presented below.

2.1.1. FMCW Radar

Frequency Modulated Continuous Wave (FMCW) radars employ a technique wherein the frequency of a continuous signal is modulated over a defined period of time. This signal is transmitted, and the antenna receives the signal reflected from the target. The delay caused by the time of flight, determined by comparing the transmitted signal and the reflected signal, is used to obtain information regarding the position and velocity of a target. In contrast to pulsed radars, FMCW radars emit continuous signals [7], [8]. The main feature of FMCW radars is their ability to measure the range and the relative velocity of targets with high accuracy and minimal range making them ideal in automotive radar and meteorological applications.

FMCW radars boast the ability to measure the target range and relative velocity simultaneously as well as the ability to make highly accurate measurements at minimal distances (the minimum measured range (R_{min}) is comparable to the wavelength of the transmitted signal transmitted). The distance between the antenna and the target (range) can be described with the following expression:

$$R = \frac{c\Delta t}{2} = \frac{c\Delta f}{2df(t)/dt}, \tag{2.1}$$

where c is the speed of light, Δt is the delay between transmitted-received signal, Δf is the observed change in frequency and $df(t)/d(t)$ is the rate of frequency shift [6].

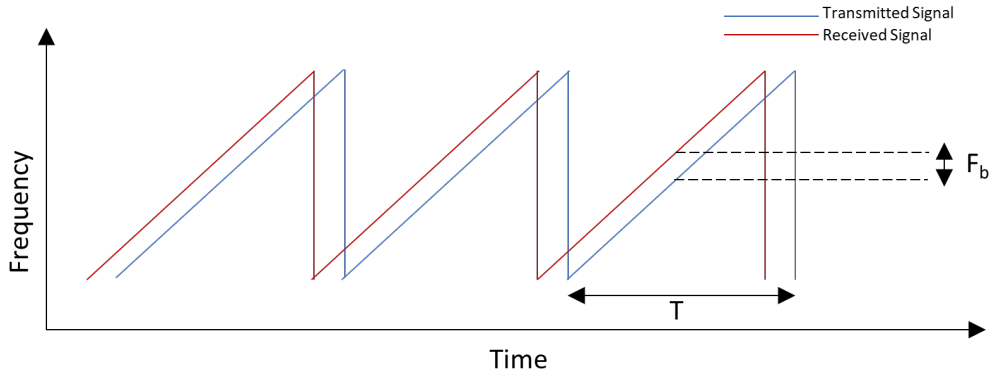

Figure 2.1: Waveform of an FMCW radar. F_b represents the beat frequency, T is the sweep time.

The primary applications of FMCW radar are in the automotive and meteorological domains. The FMCW signal has been commonly used in automotive radar applications due to its low sampling requirements and simple hardware design. The FMCW automotive radar uses a dechirping receiver where the received signal is mixed with the transmitted signal to obtain the beat signal. Subsequently, the range and velocity information of the targets are extracted from the beat signal using a two-dimensional Fourier transform [9].

A number of characteristics of radar need to be considered in order to characterize its performance and check its suitability for a particular application. Some of these are the maximum range R_{max}, range resolution ΔR, maximum unambiguous velocity v_{max}, and the velocity resolution Δv. The mathematical expressions for each of these are given below [10].

$$R_{\text{max}} = \frac{c \cdot PRI}{2} \tag{2.2}$$

$$\Delta R = \frac{c}{2 \cdot B} \tag{2.3}$$

$$v_{\text{max}} = \pm \frac{\lambda \cdot PRF}{4} \tag{2.4}$$

$$\Delta v = \frac{\lambda}{2T_i} \tag{2.5}$$

Where PRI is the pulse repetition interval, PRF is the pulse repetition frequency, B is the bandwidth, λ is the wavelength and T_i is the integration time.

The next very important application and the focus of this thesis is the use of radars for weather monitoring applications. Weather radar technologies mostly operate in the lower frequency range of the

S-band or C-band. It is selected considering the atmospheric damping and longer range. The advantage of using the FMCW method compared to other methods is the need to transmit power for FMCW radar is not large, and it is able to avoid the risk of low-accuracy data due to the use of RF components in the pulse method [11].

For various meteorological applications, different scanning strategies are utilized. Some of these are height-time mode, range height indicator (RHI), and plan position indicator (PPI). In RHI, the azimuth angle is fixed, and the radar scans in elevation, creating a vertical section of the atmosphere. On the other hand, in the PPI mode, the radar has a fixed elevation and it scans in azimuth thus creating a horizontal section of the atmosphere. Lastly, in the height-time mode, the radar is fixed in elevation and azimuth, and measurements are made as the various atmospheric processes pass through the radar beam. In this thesis the measurements are made in a similar fashion, when the radar is vertically pointed, making measurements in the zenith direction.

2.1.2. Polarimetric Radars

Polarimetric Radar makes use of the polarization properties of electromagnetic waves. It involves the use of not only the amplitude of the received signal but also the polarization state. It enables better identification of objects of interest, as different objects have different polarimetric signatures. An important concept of radar polarimetry is the scattering matrix. It describes the polarization state of the received or scattered signal with respect to the transmitted signal as shown below [12].

$$\begin{bmatrix} E_H^r \\ E_V^r \end{bmatrix} = \begin{bmatrix} S_{HH} & S_{HV} \\ S_{VH} & S_{VV} \end{bmatrix} \begin{bmatrix} E_H^t \\ E_V^t \end{bmatrix}$$

Here, E^r and E^t are the electric components received and transmitted signals, H and V represent the polarization channels of the radar and S is the scattering matrix. These polarimetric channel components are crucial in understanding different features of the target, with respect to their shape, orientation, and so on. In the next chapter, the use of this data from different polarimetric channels will be explained in detail.

2.2. Atmospheric Sensing with Radar

Radars have become increasingly popular in the field of atmospheric remote sensing due to a number of factors introduced in the previous chapter. In the context of atmospheric remote sensing, a crucial aspect that needs to be studied is the drop size distribution (DSD). DSD provides important information about the characteristics of various hydrometeors, such as raindrops or snowflakes, in the atmosphere. The knowledge of DSD can be used to measure precipitation intensity, precipitation type, rain rate, and so on. DSD provides data on the number and size of hydrometeors within a given volume of the atmosphere. It is also crucial to estimate the fall velocities of hydrometeors and it will be used in this project to estimate the vertical air velocities. The DSD can be of many forms like the exponential, gamma, log normal and so on [13]. The relation between the parameters of the drop size distributions and the radar measurables vary significantly based on the type of hydrometeor considered. many such relations for

rain, drizzle, and snow are well known in the literature [14].

When it comes to the derivations of various DSD parameters, it is also essential to understand the bounds of certain techniques based on the type of rainfall observed. The two types of rainfall considered in this thesis are stratiform and convective. Stratiform rainfall is generally characterized by a steady long duration rainfall with the presence of a bright band.Another characteristic is that after the bright band a rapid rise in the fall speeds is observed. The air velocities in stratiform rainfall are usually very low in the order of tens of cm/s. Convective rainfall on the other hand does not present with a bright band but is instead characterized with convective air turbulent air motion with different types of hydrometeors. Convective rainfall is usually short in the order of a few minutes [12]. The classification of these two rainfall types will be discussed in detail in further chapters.

2.3. PARSAX

The PARSAX radar is a high resolution, full polarimetric, S-band radar developed at Delft University of Technology. PARSAX finds application in various areas like meteorology, remote sensing and the analysis of ground based targets such as vehicles and so on. It is a full polarimetric radar, which means that it can transmit two orthogonally polarized signals at the same time, allowing it to measure all of the scattering matrix elements in the same frequency band and in a single sweep time. PARSAX also showcases a high level of RX-TX isolation (-100dB for HH polarization and -80dB for VV-ploarization)[15]. The various characteristics of PARSAX specific to this thesis are summarized below in table 2.1

Parameter	Value
Frequency	S-band(3.315GHz)
Bandwidth	50MHz
Resolution	3m
Maximum Range	150km
Sweep Time	1ms
Maximum Velocity	$\pm$22.1m/s
TX antenna	Diameter: 4.28m
	Beam width: 1.8\deg
RX antenna	Diameter: 2.12m
	Beam width: 4.6\deg

Table 2.1: Characteristics of PARSAX

3

Pipeline for Data Processing

This chapter explains the proposed data processing pipeline and the data that will be utilised in this project. It also presents the results of the initial part of the data processing pipeline pertaining to clutter and noise removal and a proposed quality check criterion.

3.1. Description of data

This section provides an overview of the dataset utilized in this project and the general structure of the NetCDF data format.

3.1.1. Dataset

The dataset utilized for this project consists of daily NetCDF files with PARSAX radar observations of vertical profiles of the atmosphere. In this project, the data recorded for the period between January 2021 and June 2021 is considered.

The data is recorded with the PARSAX radar in the vertically pointed configuration, The recorded data is organized in daily NetCDF files. NetCDF is a collection of software libraries and machine-independent data formats that enable the creation, access, and sharing of array-oriented scientific data. A typical NetCDF file is organised into separate components- attributes, dimensions, and variables. The data structure of such a file is presented in figure 3.1 [16]. The dimensions represent the physical dimensions of the data. Dimensions can have a specific size or may be defined as having an unlimited size such that it is possible to extend the file along these dimensions indefinitely. With respect to the data used in this project, the dimensions are range, Doppler, time, campaign, and zero dimension. Wherein the range dimension is of size 5100 corresponding to the number of complex samples in the coherent vertical range profile, the Doppler dimension has a size of 512, the campaign dimension is of size 100, and the time dimension is the unlimited dimension.

Attributes are essentially metadata, serving as descriptive markers that provide crucial information

about the dataset. Global attributes provide information pertaining to the date of measurement, institution, measurement instrument name, and so on. A detailed description of all attributes is presented in appendix A. Besides the global attributes, each variable possesses attributes that further describe the variable. These include data type, measurement units, and comments that provide further insight into the variable.

Variables contain information on the data recorded by the PARSAX radar. They may be classified into a few categories for ease. Variables containing the geographic position data of the radar are latitude, longitude, and altitude. Variables that contain the measurement specifics are the current day, the current time, and the current campaign. Variables like antenna mode, radar frequency, bandwidths of different polarization channels, transmitted power, antenna elevation, azimuth, and polarization provide the specifications of the radar system in the measurement period. The moments of the Doppler spectrum- reflectivity, Doppler velocity, and spectral width for the different polarization channels are present as a function of two dimensions, range and time. A detailed description of all the variables is provided in appendix A. These moments will be processed and will be utilized in all further algorithms implemented.

MATLAB has a plethora of tools for reading, extracting, and altering data from NetCDF files. For this objective, two techniques can be considered: employing high-level Matlab functions or using low-level netCDF library functions. The low-level functions in the netCDF library package offer far more capability than the high-level ones. A comprehensive set of functions enables access to and manipulation of several aspects of NetCDF data. Obtaining information from the NetCDF file, reading and writing data, creating variables, renaming dimensions, attributes, variables, sampling between particular intervals, and so on are some of them. Owing to the better control that these functions provide and their faster execution times, the low-level functions are preferred over the high-level functions.

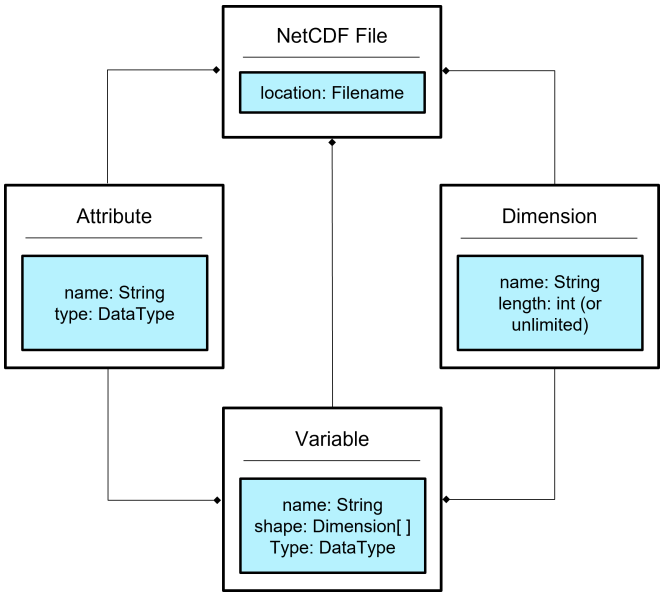

Figure 3.1: Data model of a NetCDF File

3.2. Data Processing Pipeline

One of the most crucial aspects of accurate rainfall and wind velocity estimation is having reliable and high-quality radar data. This is significant because inaccurate data or data with certain deficiencies can lead to erroneous estimates. The measured vertical profiles are affected by thermal noise and clutter. The clutter mainly appears in the form of echoes from biological targets (like birds and insects), clear sky reflections, and miscellaneous clutter. It is essential that the data being utilized in the further steps i.e. classification and vertical air velocity estimation are free from these effects which would ensure more accurate estimates. To achieve this goal a data processing pipeline is proposed as shown in figure 3.2.

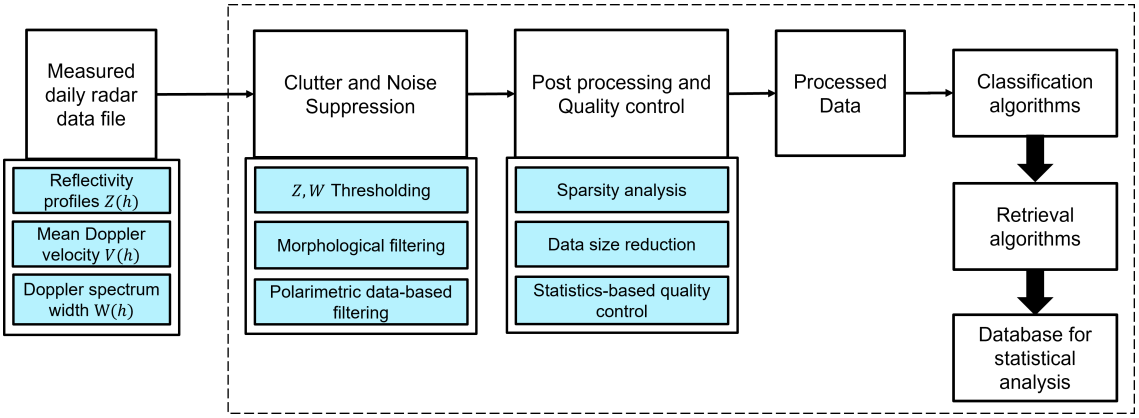

Figure 3.2: Data processing pipeline

This data processing pipeline plays a crucial role in transforming raw measured data to enhance its suitability for further analysis. It ensures data integrity, reliability, quality, and efficient usability. This is achieved by leveraging a number of techniques, all of which are detailed below.

3.2.1. Clutter and Noise Suppression

The vertical profiles of reflectivity, mean Doppler velocity, and Doppler width are considered. The clutter removal is done by creating a target mask for the desired meteorological targets which are precipitation, clouds, ice particles, and so on. By utilizing this, the echoes from non-meteorological targets (like birds and insects), clear sky reflections, and erroneous echoes are removed from the data. The target mask is created by employing the following methods.

Reflectivity and Doppler width-based filtering: The first method involves imposing thresholds on the upper and lower limits of the observed reflectivity, and Doppler width. These thresholds are selected such that they prove to be good factors in discriminating between the desired signal and clutter. The size of raindrops is limited; hence, the maximum observed reflectivity can be limited to $+60$ dBZ [17]. However, after experimental analysis of the dataset used in this project, it was observed that the maximum reflectivity may be limited to $+40$ dBZ, while the lower bound for reflectivity is set to -15 dBZ. The procedure for this analysis has been explained in detail at the end of this section.

The distinction between clutter and meteorological targets can be further discerned by considering the Doppler spectral width as an additional distinguishing characteristic [18], [19]. Different me-

teorological phenomena exhibit distinct ranges of Doppler spectrum widths and the impact of non-meteorological clutter leads to further variations. With clear air, the values for the Doppler spectrum widths may not exceed 7 m/s, which are already considerably higher and are attributed to biological scatterers. Under stratiform and storm-like rain conditions, with reflectivity levels ranging from 20 to 40 dBZ, the theoretical values established by Doviak and Zrinc [18], complemented by the empirical findings of [20], consistently indicate that the spectrum widths remain confined to an approximate maximum of 3.8 m/s. Following thorough experimental analysis, specific Doppler width thresholds are determined, setting the upper bound at 3 m/s and the lower bound at 0 m/s.

Polarimetric feature-based filtering: The second method utilizes the data from the different polarization channels. Polarimetric features like differential reflectivity and linear depolarization ratio can be used to distinguish between the desired meteorological targets and clutter[21],[22]. Differential reflectivity(Z_DR) can be mathematically represented as the ratio of the reflectivity from the horizontally polarized channel and the vertically polarized channel as shown in equation 3.1 [23].

$$Z_{DR} = 10 \cdot \log\left(\frac{Z_{HH}}{Z_{VV}}\right) \tag{3.1}$$

Z_{DR} can be used as an indicator of the shape of the target and the values measure the oblateness of the targets. Z_{DR} of the observed feature is greater than 1, it signifies that the feature possesses a wider horizontal extent compared to its vertical extent. Conversely, when the ratio falls below 1, it indicates that the feature exhibits greater vertical elongation in comparison to its horizontal extent. When the ratio approaches unity, the feature can be approximated as having a near-spherical shape. As the radar measurements are made in the zenith direction the shape of the raindrops can be approximated to be spherical. Typical values for the Z_DR for rain range between 0 and 3dB[23]. Considering this and the results from the experimental analysis of data the threshold for the differential reflectivity is limited to 5dB. The vertical profile of Z_DR is presented in figure 3.3. It can be clearly observed that the magnitude of Z_DR is largely close to 0dB. Figure 3.4 shows a plot of Z_HH vs Z_VV where the outliers with Z_DR>5db can be clearly visualised.

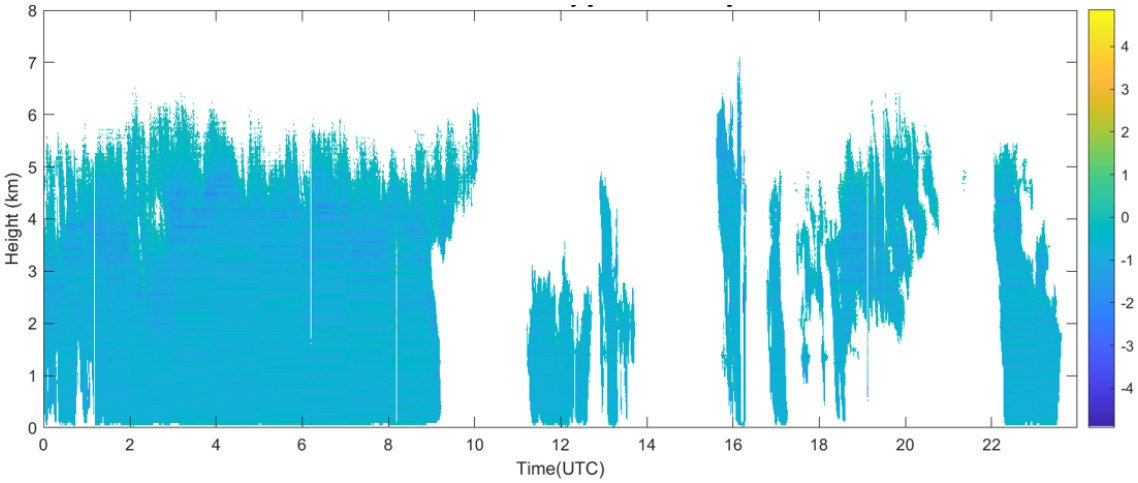

Figure 3.3: Vertical profiles of differential reflectivity

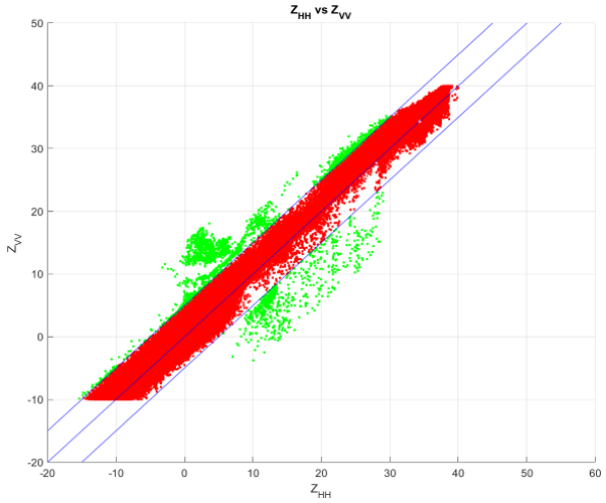

Figure 3.4: Visualization of outlier data

The second polarimetric feature considered is the linear depolarization ratio (LDR). LDR occurs as a result of the depolarization properties of targets. The LDR is mathematically represented as the ratio of the cross-polarized components(Z_HV, Z_VH) to the co-polarized components(Z_HH, Z_VV) as shown in equation 3.2.

$$LDR_{VV,HH} = 10 \log \left(\frac{Z_{HV,VH}}{Z_{VV,HH}} \right) \tag{3.2}$$

The magnitude for the cross-polarized measurements is much smaller than that of the co-polarized measurements for meteorological targets [24]. Hence, they exhibit much lower values of LDR as compared to biological or other non-meteorological targets. The criteria proposed in the literature to distinguish between meteorological targets and non-meteorological targets was to limit the LDR to -5dB [22], [24]. However experimental analysis of the data showed that this threshold caused portions of the desired precipitation and cloud regions to be removed. Hence the optimum threshold was determined to be -10dB. The vertical profile of the LDR is presented in figure 3.5. The highest level magnitudes are observed around the bright band as a result of the depolarization properties of ice crystals and melting snowflakes [22].

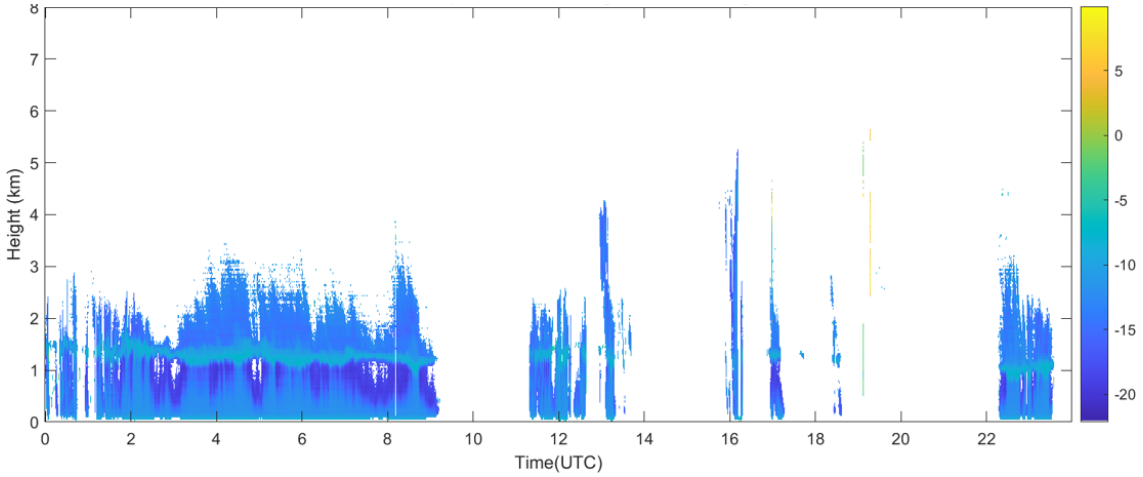

Figure 3.5: Vertical profiles of linear depolarization ratio

Morphological filtering: The third approach employed for creating the target mask involves the utilization of morphological filtering, a widely used technique that is typically utilized to enhance the quality of radar data by mitigating the impact of noise and enhancing specific features of interest. Morphological filtering specifically employs a morphological operation known as opening, which effectively eliminates small and isolated features, commonly referred to as speckle noise, from the radar image while preserving the larger, more significant features that encompass the desired radar data [25].

Speckle noise refers to isolated range bins within the radar image that may contain valid data but are surrounded by adjacent bins that contain no data [19]. Through the application of morphological filtering techniques, these isolated data points or speckle noise, are effectively eliminated from the radar image, thereby enhancing the overall quality and clarity of the data. By employing this method, the obtained results are more reliable and accurate, making the data more suitable for subsequent interpretation and analysis. The overview of the morphological filtering operation is presented in figure 3.6 and is explained elaborately below.

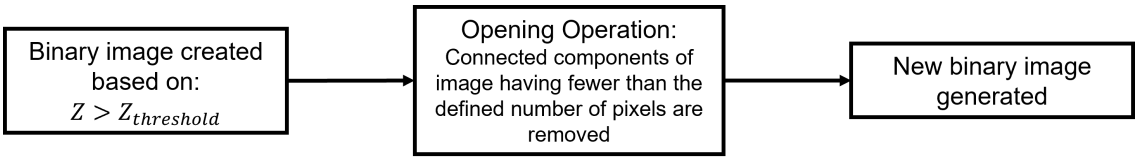

Figure 3.6: Morphological filtering flowchart

The morphological operation of opening takes place in the following way. The first step is to generate a binary image containing the region of interest. In this case, this region is defined by selecting all data bins that have a reflectivity higher than -15dBZ. Once this binary image is generated, the morphological filter evaluates each data bin and its adjacent neighbours. All the connected components (data bins) of the newly created binary image that have fewer than the defined number of data points are set to have no data. In this scenario, this defined number is set to 200. Following this operation, a new binary image with minimal impact of speckle noise is generated which can be used to generate the target mask for the final step of filtering the data.

As introduced above, the next crucial step carried out is the experimental analysis of the data, to obtain optimum thresholds for all the filtering operations. This comprehensive analysis involved the examination of a collection of six distinct data files sourced from different time periods throughout the year, effectively capturing a wide range of rainfall patterns including various types and intensities. Moreover, these selected data files were specifically chosen to reflect diverse clutter characteristics in terms of both degree and nature. In addition to this, these files encompassed varying degrees of sparsity within the daily dataset, the need for this and the mitigation strategies are discussed further in the next section. It is thereby reasonable to assume that these selected data files can be deemed to be representative of the broader dataset under consideration. This analysis was carried out by initially applying the default threshold values to generate the target mask and then modifying them to obtain the optimum clutter removal without the loss of any usable data. Following this, all the thresholds and associated parameters were optimized and selected as mentioned previously. The target mask generated based on the three techniques; reflectivity and Doppler width based-filtering, polarimetric

feature-based filtering and morphological filtering is presented below in figure 3.7 and the unfiltered data is presented in figure 3.8. This target mask is now applied to the raw data and the processed data is presented in figure 3.9.

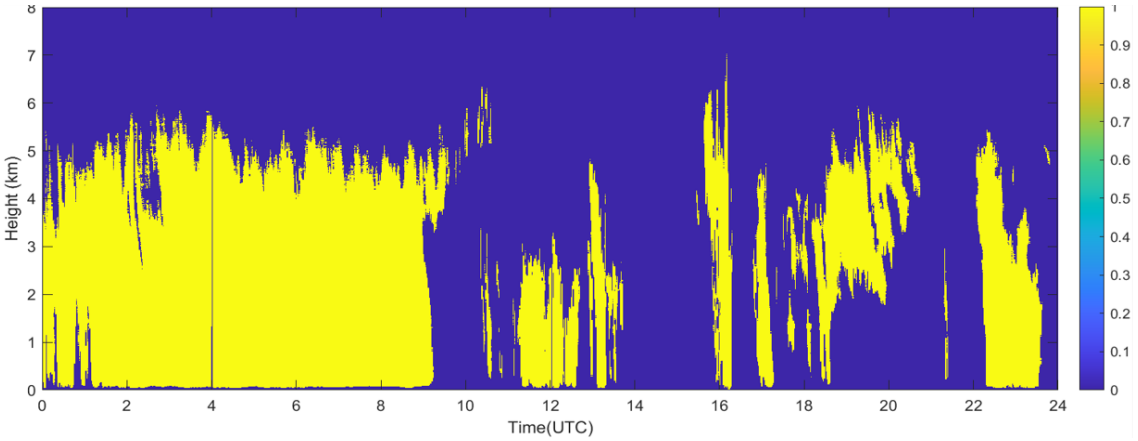

Figure 3.7: Target mask generated using all three filtering techniques

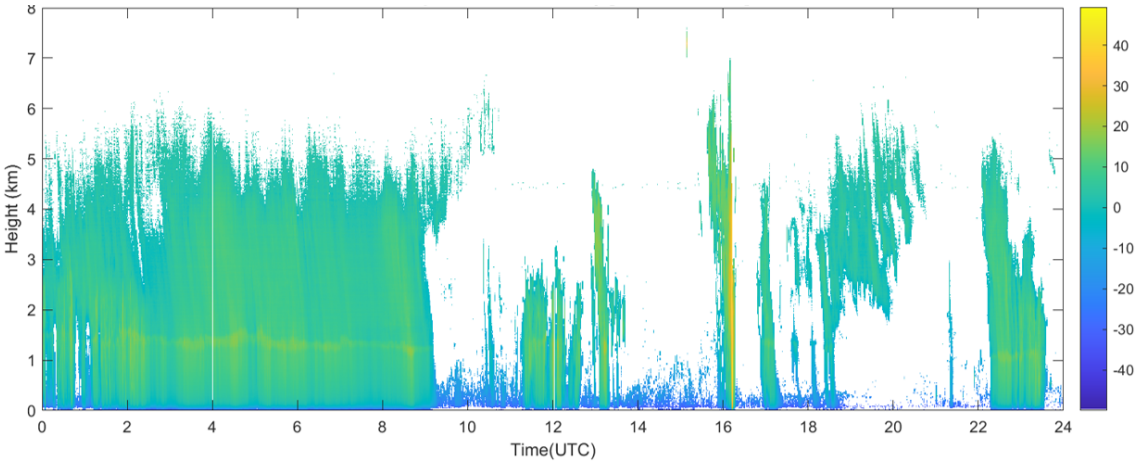

Figure 3.8: Unprocessed vertical profiles of reflectivity

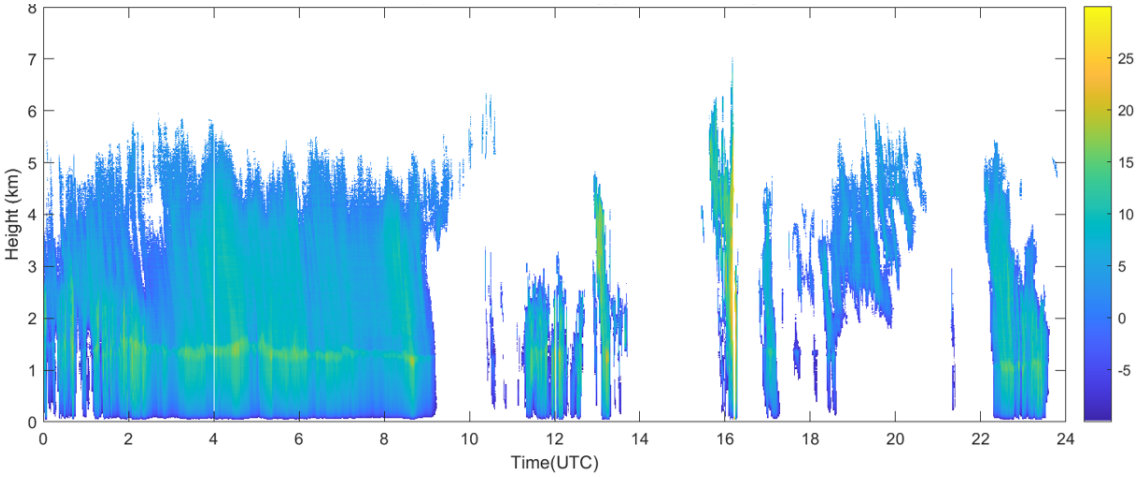

Figure 3.9: Processed vertical profiles of reflectivity

3.2.2. Post-processing and quality control

The next step in the data processing pipeline is the post-processing and quality control of the data. It involves three tasks, the first task being sparsity analysis, followed by the reduction of data size, and lastly is the quality control step which is done by considering certain statistics of the data.

Sparsity Analysis: The data files involved in this project are extremely large and yet there are significant portions of the recorded daily files that are either innately missing, have very little or no usable data or have had portions of noisy data removed after the noise and clutter removal operation. By doing the sparsity analysis of this data, it is possible to remove such portions of the data to further increase the quality and reliability of the data. One such example is shown in figure 3.10.

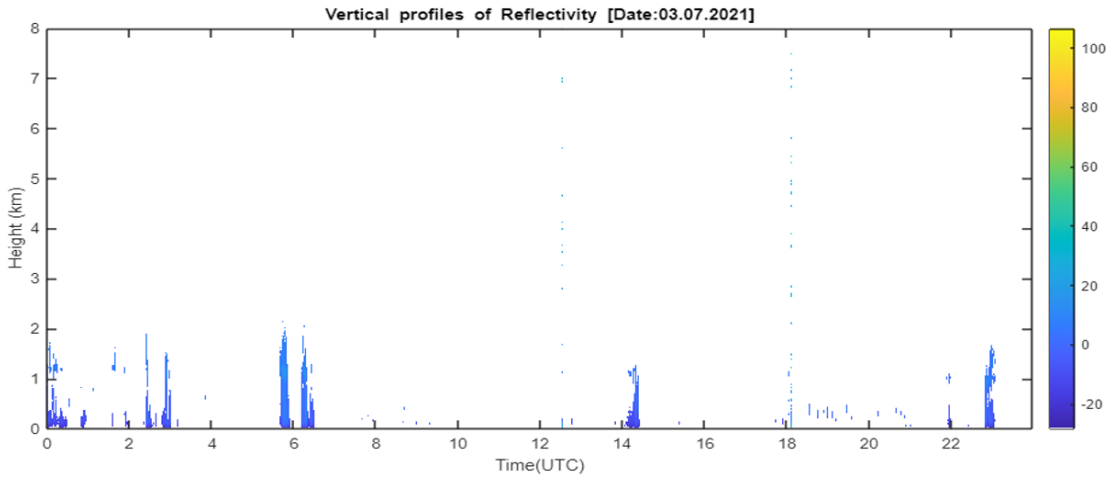

Figure 3.10: Daily data file containing sparse data

It is evident from figure 3.10 that approximately an hour of usable data and besides that all of the remaining data is fairly unreliable and would cause errors in further steps of the project hence the values in this portion of the data have been set to no data. As will be discussed further, the data from this point on will be processed in segments, and therefore such segments containing sparse measurements will not be utilised in any further analysis.

Spatial and Temporal Averaging: As one of the important goals of this project is to analyze large-scale data, it is crucial that the data processing be as efficient as possible. For this purpose, the data is average in the time and range domain. By doing this the range resolution and the temporal resolution is degraded from 3.3m and 0.5s respectively to 33m and 30s respectively. These new spatial and temporal resolutions provide the details of the selected volume of atmosphere in sufficient detail and are reasonably small enough that the atmospheric parameters can be considered to not vary significantly in such an averaged data.

Quality Check Criterion: The quality and reliability of data being utilized in this project are paramount and hence, a quality check criterion is proposed which is based on the correlation between the horizontal and vertical polarized channels. As mentioned earlier, due to the configuration of the radar, i.e. the measurements being taken in the zenith direction, the shape of the drops is assumed to be spherical and hence a high degree of correlation is expected between the two polarization channels. This correlation is presented in equation 3.3.

$$\rho = \frac{\sum Z_{VV_i} Z_{HH_i}}{\sum (Z_{VV_i})^2 (Z_{HH_i})^2} \tag{3.3}$$

The correlation is analysed as a function of the height as shown in figure 3.11. It can be observed that there is a high correlation between the HH and the VV polarization channels across the entire profile except at very low altitudes. This may be attributed to the artifacts introduced by the interference in the radar itself as well as certain disturbances caused in the atmosphere due to the building where the PARSAX radar is located. Hence the data up to the altitude of 100m is discarded.

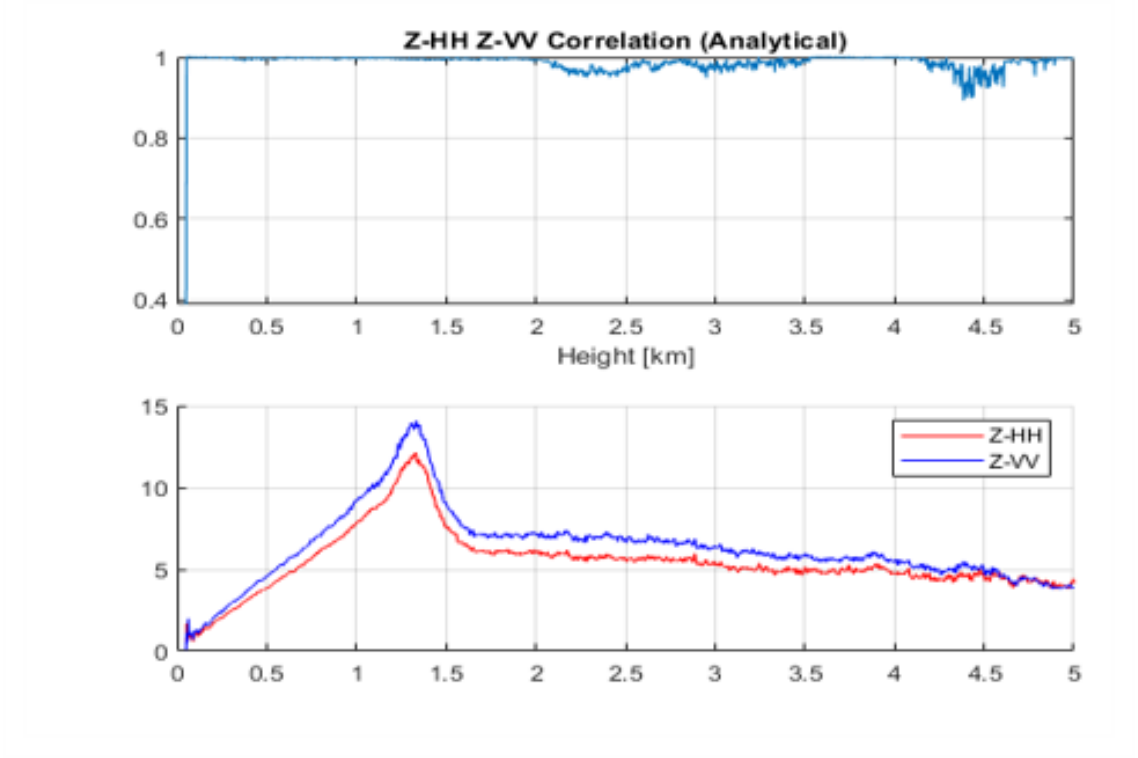

Figure 3.11: Correlation between HH and VV channel data

3.3. Results

After having implemented the clutter and noise suppression operations, and having carried the post-processing and quality control steps, the processed and now high-quality and reliable data consisting of the vertical profiles of the reflectivity, mean Doppler velocity and the Doppler spectrum width are presented in the Figure 3.12. It is also found that the data processing pipeline is able to efficiently process the data files for all six months.

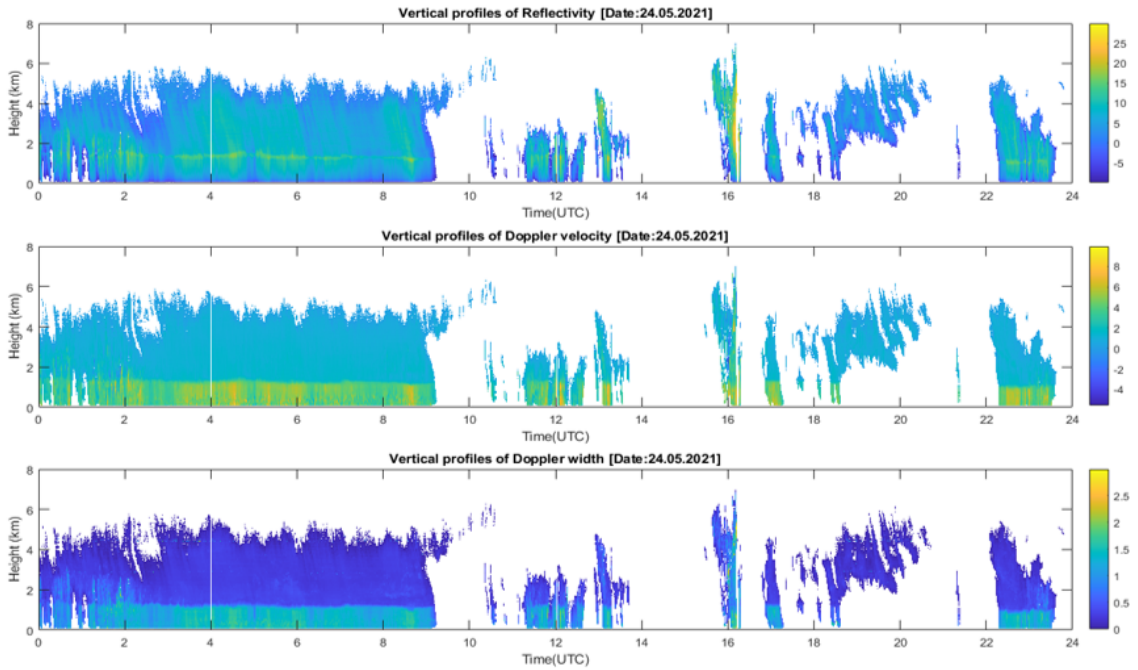

Figure 3.12: Processed vertical profiles of reflectivity, Doppler velocity, and Doppler width

3.4. Conclusions

This chapter detailed the data processing pipeline that has been proposed. The initial steps within the pipeline that include clutter and noise suppression and deriving the desired meteorological target using three different techniques are presented. Two post-processing techniques employed to make the data processing efficient and mitigate the possibility of errors induced due to improper data have been demonstrated. Along with this a quality control criterion has been developed and implemented. The final processed data is presented and the performance of all the aforementioned techniques is validated. The processed data is highly reliable. In conclusion, each step in the data processing pipeline is interconnected and essential for accurate and valuable data processing and analysis. Following this, the next chapter discusses how this data will be utilised for the purposes of classification of rain types and the regions of precipitation.

4

Classification Algorithm

In this chapter, the developed algorithm for the classification of rain types and the regions observed in the vertical profile of the atmosphere is presented. This chapter also discusses the relevant literature, the implementation of this algorithm, and the results obtained.

4.1. Overview of the classification algorithm

4.2. Review of literature

Within the literature, there are a number of techniques and algorithms proposed for the classification of rainfall into two major types, stratiform. Most of these techniques utilize one or more radar observables to establish certain criteria to distinguish between the two types of rainfall. One commonly used distinguishing factor between the two types is the occurrence of a bight-band layer. Many studies have proposed criteria to determine bright bands and consequently classify the rain types [26]. Table 4.1 provides a summary of some of the proposed classification algorithms.

Reference Study	Basis of Classification	Classification
Williams, et al. [27]	Presence of melting layer at medium altitudes (~3km), and turbulences at higher altitudes (~7km). Utilizes Doppler width.	Stratiform/ convective
White, et al. [28]	Presence of a bright band; determined by the simultaneous decrease in reflectivity and an increase in the Doppler velocity. Utilizes reflectivity and Doppler velocity.	Stratiform/ convective

Thurai, et al. [29]	Presence of a bright band; determined by several relations between peak reflectivity and mean reflectivity.Utilizes only reflectivity.	Stratiform/ convective
Gil-de-Vegara, et al.[30]	Presence of a bright band; determined using threshold set for the increase in the Doppler velocity. Utilizes only Doppler velocity.	Stratiform/ convective
Rico-Ramirez, et al. [31]	Presence of a bright band determined using the peak reflectivity and the gradient of reflectivity within a region around the altitude of peak reflectivity.	-

Table 4.1: Overview of classification schemes presented in literature

4.3. Classification criteria

The selection of the classification criteria for this project is based on a comprehensive review of the existing literature, wherein the classification framework proposed by Thurai et al. has been identified as the most appropriate. In their work, Thurai et al. established a classification method that focuses on stratiform and convective rainfall differentiation through the detection of a distinctive meteorological phenomenon known as the bright band. The presence of the bright band is determined by considering multiple relationships between peak reflectivity and mean reflectivity, which serve as key indicators in discriminating between the two rainfall types. Specifically, the bright band classification criterion emphasizes the utilization of reflectivity as the primary distinguishing feature in this context. If the criteria to detect the presence of stratiform rainfall are met, the rainfall is classified as stratiform and if not, convective. The criteria are as follows. The difference between peak reflectivity and the mean reflectivity below the bright band should be greater than 1dBZ. The difference between peak reflectivity and the reflectivity 1km above the bright band should be at least 2dBZ. Lastly, the peak reflectivity should be greater than the maximum reflectivity below the bright band [29]. These criteria are summarized below.

Algorithm 1: Detect Rainfall Type

Data: Peak Reflectivity (Z_{peak}), Mean Reflectivity below Brightband (Z_{mean}), Reflectivity 1km above Brightband ($Z_{1\text{km}}$), Maximum Reflectivity below Brightband (Z_{max})

Result: Rainfall Type (Stratiform or Convective)

if $(Z_{peak} - Z_{mean})$ > 1 dBZ ***and*** $(Z_{peak} - Z_{1km}) \geq$ 2 dBZ ***and*** (Z_{peak}) > (Z_{max}) **then**
    return "Stratiform"
return "Convective"

These characteristics can be observed in the vertical reflectivity profiles as shown in figure 4.1

In order to classify the various regions in the vertical profiles of the atmosphere, mainly divided into four classes; rain, clouds, melting layer, and absent data bins. Hence these regions are characterized by the type of hydrometeors present in them. The classification of these regions is also done based on the boundaries of the bright band. The region below the bright-band is classified as rain. The bright-

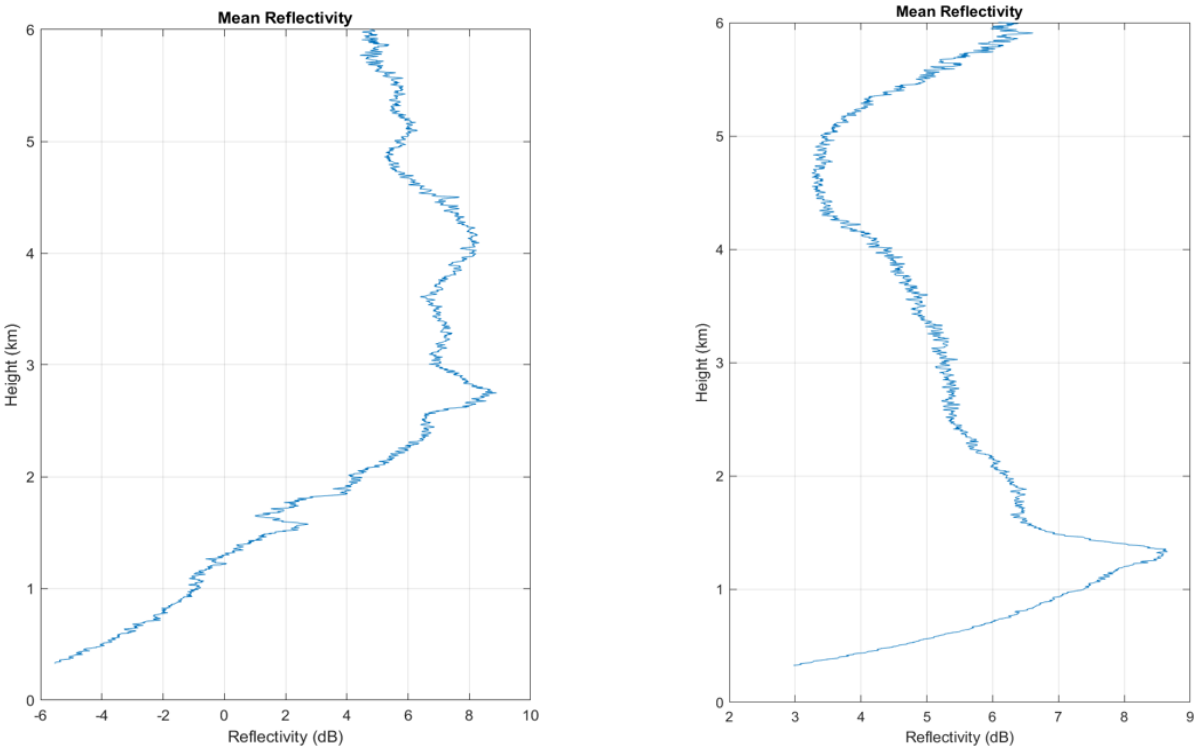

(a) Convective rainfall

(b) Stratiform rainfall

Figure 4.1: Vertical reflectivity profile for convective and stratiform rainfall events

band signifies the melting layer or the mixed phase layer where the ice crystals are melting into water or larger water droplets are forming. The region above the bright-band consists of clouds and ice particles and are hence classified as such. The results of both these classifications are presented in the next section.

4.3.1. Bright-band detection algorithm

The algorithm used to detect the bright-band is a modified version of the algorithm proposed by Rico-Ramirez et al which utilizes only the reflectivity. The algorithm proposed in this utilizes the reflectivity as well as the mean Doppler velocity and the Doppler spectrum width. The algorithm involves first identifying the peak reflectivity and the altitude at which this peak reflectivity occurs in a single vertical profile of reflectivity. Then arbitrary boundaries are selected 500m above and below the altitude of maximum reflectivity. This is selected such that is surely beyond the upper and lower bound of the bright-band [31]. Following this, the gradient of reflectivity is calculated in this newly defined region is calculated. The reflectivity sharply increases in the bright band and therefore the altitudes with the highest numerical gradient above and below the peak reflectivity altitude are defined as the upper and lower bounds of the bright band. To further improve the accuracy of the lower bound of the bright band the Doppler velocity and the Doppler width are used. The lower bound of the bright band layer is the point at which the rainfall commences, hence there is an abrupt jump in the mean Doppler velocity and there is a widening of the Doppler spectrum width. This change in these two parameters is used to obtain more accurate bright band bounds. The vertical profile of reflectivity during a typical stratiform

rainfall event that exhibits a bright band is shown below in figure 4.2

Algorithm 2: Bright Band Detection Algorithm

Data: Vertical Profile of Reflectivity
Result: Upper and Lower Bounds of the Bright Band
1 Identify the peak reflectivity: $Z_{\text{peak}} = \max(Z)$;
2 Identify the altitude of the peak reflectivity: $A_{\text{peak}} = \arg\max(Z)$;
3 Define the region of interest: $A_{\text{upper}} = A_{\text{peak}} + 500\,\text{m}$, $A_{\text{lower}} = A_{\text{peak}} - 500\,\text{m}$;
4 Calculate the gradient of reflectivity in the region of interest: $G(A) = \frac{dZ}{dA}$;
5 Find the altitudes with the highest gradient above and below A_{peak} as the upper and lower bounds of the bright band: $A_{\text{upper\_bound}} = \arg\max(G(A))$, $A_{\text{lower\_bound}} = \arg\max(G(A))$;
6 Use Doppler velocity and Doppler width to refine the lower bound of the bright band;
7 Detect rainfall commences based on Doppler velocity and Doppler width: $A_{\text{rainfall\_start}} = \text{DetectRainfallStart}(V, W)$;
8 **return** A_{upper_bound}, A_{lower_bound}

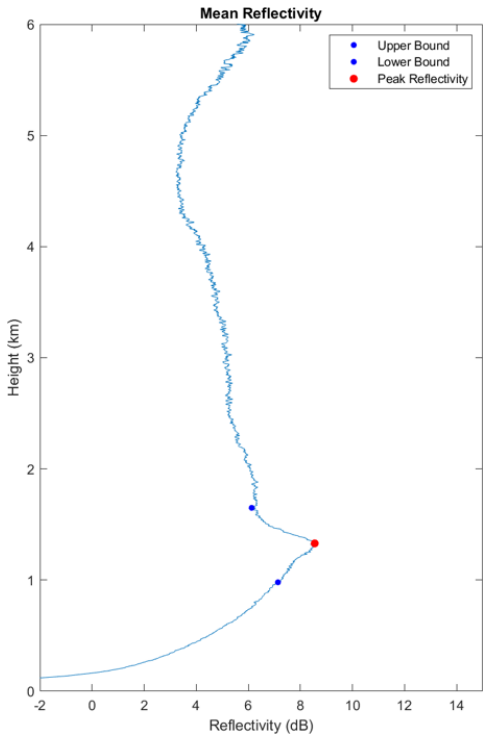

Figure 4.2: Vertical profile of reflectivity with BB boundaries

By using this algorithm, the bright boundaries for a stratiform rain event are presented below in figure 4.3.

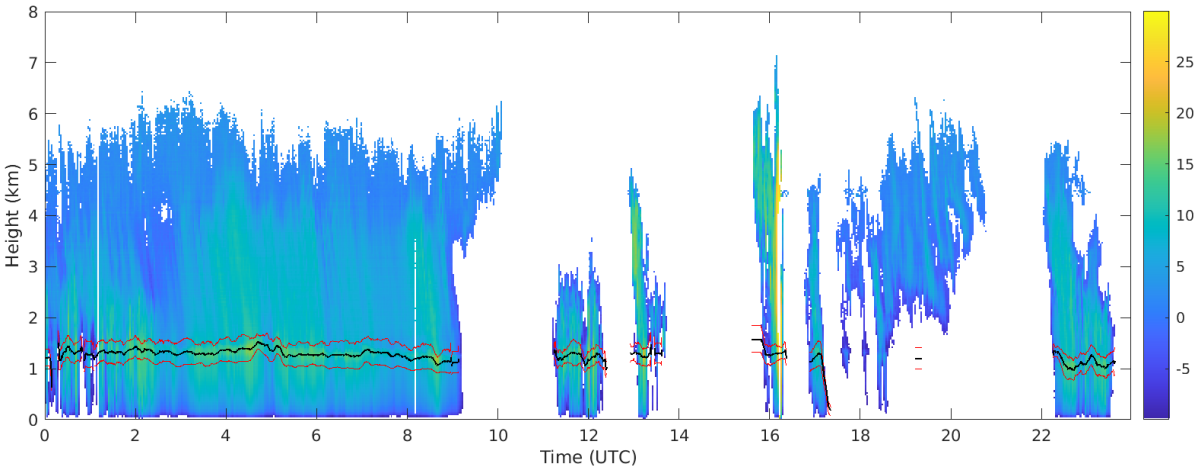

Figure 4.3: Vertical profiles of reflectivity with BB boundaries for an entire precipitation event

4.4. Classification results

By using the classification criteria and the bright band detection scheme mentioned above, the obtained classification results are presented below.

4.4.1. Classification of rainfall types

The classification algorithm was able to successfully classify stratiform and convective rainfall events. The vertical profiles of reflectivity for two such events are shown below.

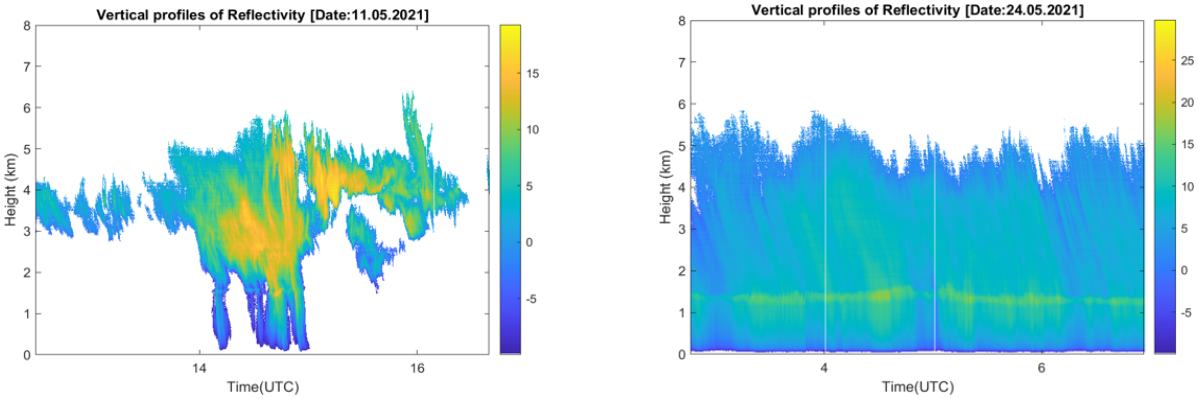

(a) Convective rainfall

(b) Stratiform rainfall

Figure 4.4: Vertical reflectivity profile for convective and stratiform rainfall events

4.4.2. Classification of hydrometeor classes in the vertical profile of the atmosphere

After having detected the bright-band or by considering the changes in the mean Doppler velocity and Doppler spectrum width, the various regions are calculated as shown in figure 4.5.

Following this analysis with the data of six months was carried out. The days within the recorded data during which precipitation presented with a distinct bright-band were considered to see the variation in altitude of this bright band across these six months. It is evident from figure 4.6 that the occur-

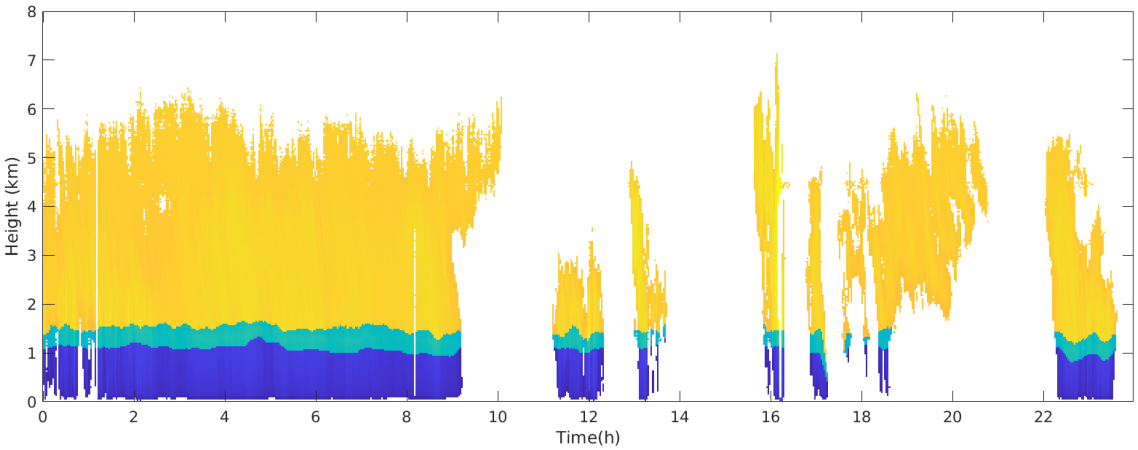

Figure 4.5: Vertical profiles of reflectivity with regions classified

rence of the bright band varies through the year. The altitude at which it occurs increases as the season changes from winter in January-February, to spring and early summer in March-June. Despite this observation, it is also possible that different weather conditions, with respect to temperature humidity and so on might further affect the occurrence of this melting layer.

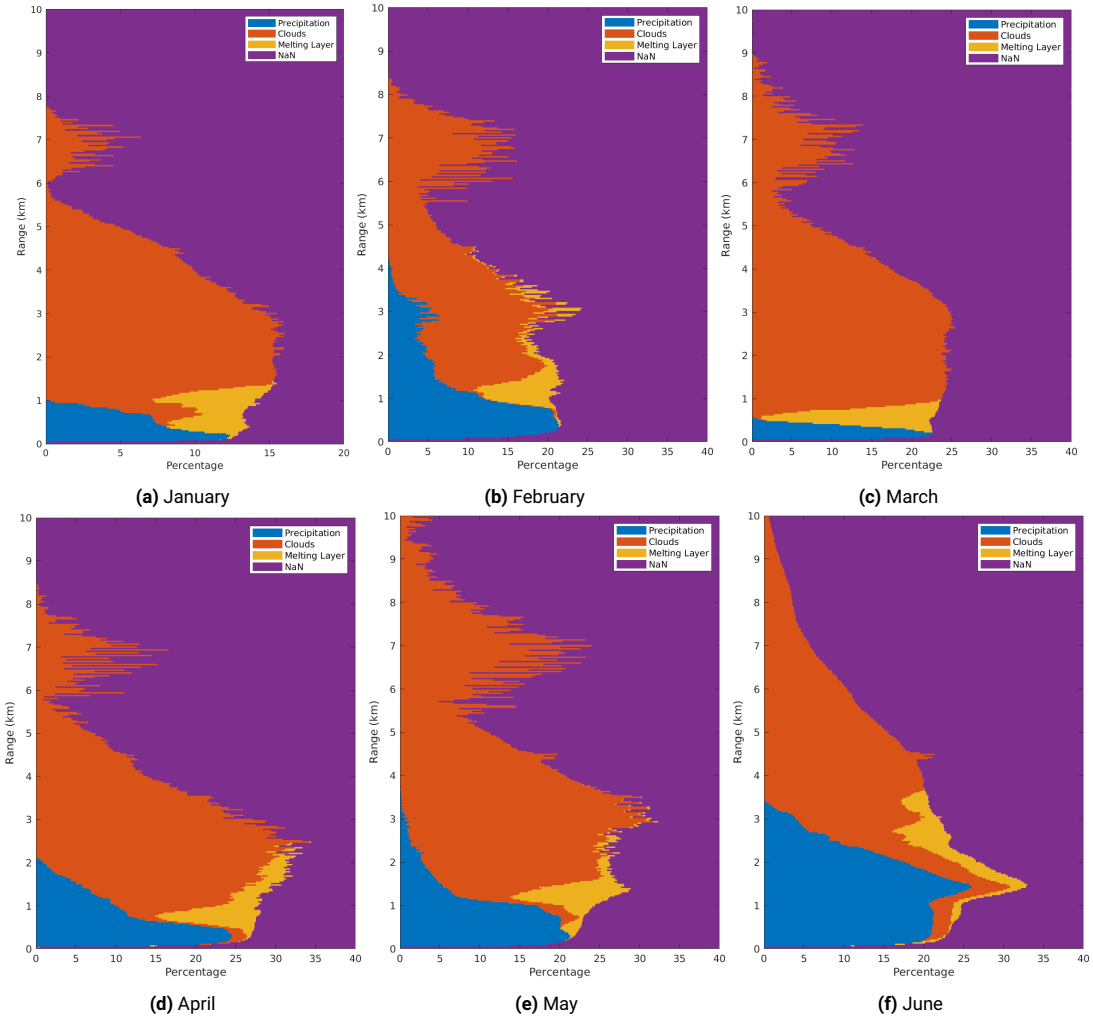

(a) January **(b)** February **(c)** March

(d) April **(e)** May **(f)** June

Figure 4.6: Variation in the altitude of various classes across six months

4.5. Conclusions

This section detailed the classification algorithm used for the classification of the types of rain i.e. stratiform and convective and the classification of the regions in the atmosphere characterized by the type of hydrometeors i.e. rain, clouds, and melting layer. The proposed bright-band detection scheme was implemented and the results are presented. The combined classification algorithm was able to successfully able to carry out the classification tasks as reported in the results. Subsequently, the dataset containing information pertaining to the specific rainfall type and hydrometeor classes of interest will be employed in the algorithms developed for the purpose of retrieving estimates of the vertical air velocities in the next chapter.

5

Retrieval of Vertical Air Velocity

This chapter describes in detail the algorithm used to retrieve the vertical air velocity. Initially, the review of literature is presented, after which the proposed algorithm itself is discussed, the criteria for the quality of the retrievals are explained and lastly, the results are presented.

5.1. Review of Literature

The retrieval of vertical air velocity from radar measurements is a very interesting problem. There are many different methods that have been proposed in the literature. For the scope of this thesis, the methods that utilize the spectral moments to derive the air velocities are the only ones that have been considered. The spectral moments method is a method for retrieving the DSD and mean Doppler velocity of hydrometeors in clouds from radar measurements. Many definitions of the drop size distribution and ways to derive the parameters for these have been proposed in the literature [13]. The most common definition of the drop size distribution is the exponential distribution first proposed by Marshall and Palmer [32]. This definition used two parameters to describe the distribution (N_0 and D_0) but the N_0 parameter is fixed.

$$N\left(D\right) = N_0 e^{(-\Lambda D)} \tag{5.1}$$

It was shown by Waldvogel that N_0 is not constant but varies [33]. Following this a gamma distribution was introduced in [34], which utilized three parameters, N_0, D_0 and μ.

$$N\left(D\right) = N_0 D^{\mu} e^{(-\Lambda D)} \tag{5.2}$$

These three parameters can be considered as three independent parameters or a constrained gamma function can be used wherein μ is a constant or μ is a function of D_0 as proposed by [35]. The summary of various DSDs is presented in figure 5.1 In this thesis, the exponential distribution is considered and a relation between spectral moments and the fall velocity of raindrops is established.

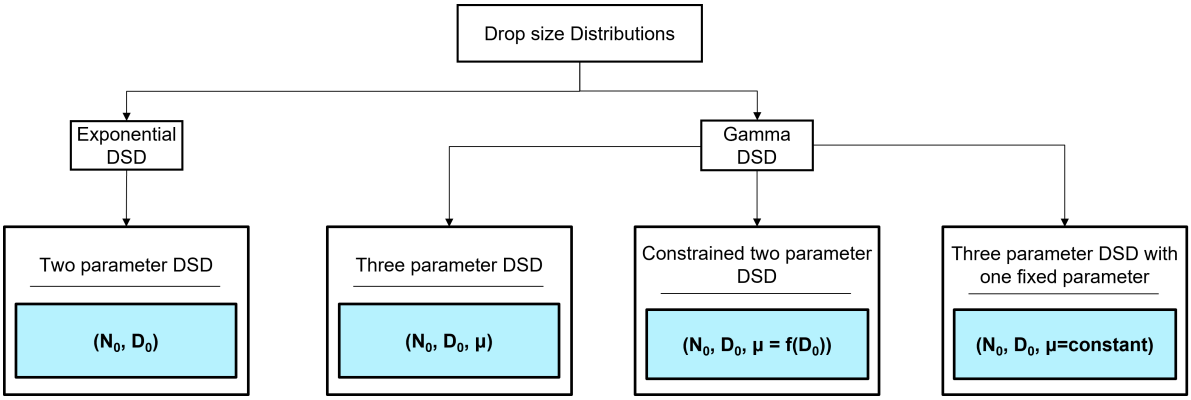

Figure 5.1: Overview of various drop size distributions

5.2. Vertical Air Velocity Estimation

In this section, the methods employed to estimate the terminal velocities of raindrops are presented. The measured mean Doppler velocity is a result of contributions by both the vertical air velocities and the terminal fall velocities of raindrops or any other hydrometeors. The proposed algorithm aims to estimate this vertical velocity correction.

5.2.1. Marshall Palmer (Exponential) Distribution

The Marshal-Palmer distribution as shown in equation 5.3[32], is considered to initially calculate the terminal fall velocity of raindrops. In the following equation, N_0 is the intercept parameter, λ is the slope parameter and D is the diameter of the raindrops.

$$N\left(D\right) = N_0 e^{(-\Lambda D)} \tag{5.3}$$

An approach proposed by Pinsky (2023) [36], [37] is considered within the further analysis. This involves relating the spectrum width of the Doppler spectrum (σ) to the terminal fall velocity of raindrops. The zeroth (reflectivity (Z)), first (mean Doppler velocity(v)), and second moments of the Doppler spectrum are considered. The spectrum width can be calculated from the first and the second moment. These relations are shown in equations 5.4, 5.5, 5.6 respectively.

$$Z = \int D^6 N(D) dD = \frac{\Gamma(7) N_0}{\Lambda^6} \tag{5.4}$$

$$\langle v \rangle = \frac{\int V(D) D^6 N(D) dD}{\int D^6 N(D) dD} \tag{5.5}$$

$$\sigma^2 = \left\langle v^2 \right\rangle - \left\langle v^2 \right\rangle = \frac{\int V^2(D) D^6 N(D) dD}{\int D^6 N(D) dD} - \left[\frac{\int V(D) D^6 N(D) dD}{\int D^6 N(D) dD} \right]^2 \tag{5.6}$$

In the above equations, $V(D)$ is given by Atlas(1973) [14],

$$V(D) = V_0 (1 - \alpha e^{(-\beta D)}) \tag{5.7}$$

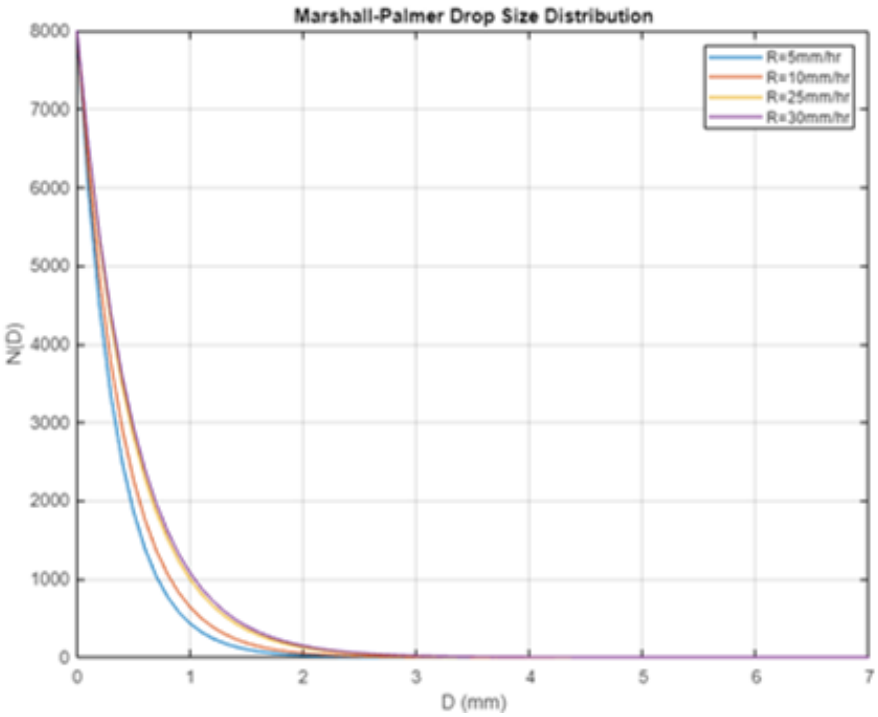

Figure 5.2: Exponential DSD

where $\alpha = 1.07, \beta = 600m^{-1}, V_0 = 9.65m/s$

Using equations 5.4 and 5.7 , the equation for the square of the spectrum width becomes the following.

$$\sigma^2 = {V_0}^2 \left[1 - \frac{2\alpha}{(1+\beta/\Lambda)^7} + \frac{\alpha^2}{(1+2\beta/\Lambda)^{14}}\right] - {V_0}^2 \left[1 - \frac{\alpha}{(1+\beta/\Lambda)^7}\right]^2 \tag{5.8}$$

$$\sigma^2 = {V_0}^2 \alpha^2 \left[\frac{1}{(1+2\beta/\Lambda)^7} - \frac{1}{(1+\beta/\Lambda)^{14}}\right] \tag{5.9}$$

A fourth-order polynomial approximation is proposed by Pinsky(2023) [36], [37] for the relation between the fall velocity of the raindrops and the spectrum width which is given by 5.10. This relation can be seen in figure 5.3

$$\langle v \rangle (\sigma) = \begin{cases} 7.4452\sigma^4 - 16.4197\sigma^3 + 12.5107\sigma^2 - 0.3607\sigma + 0.1555 & \text{for } \sigma < 1.2761 \\ 6.0144 & \text{for } \sigma \geq 1.2761 \end{cases} \tag{5.10}$$

The use of this approximation introduces a problem in the retrievals, as the applicability of the approximation is limited by the value of sigma. By analyzing multiple data files from the dataset, it is found that only 74% data points can be used for this approximation as they showcase a spectrum width of less than 1.217m/s. If only the region of precipitation is considered, the applicability is further reduced to 34%. This leads to all such data points being assigned the fall velocity of 6m/s which leads to erroneous estimation of the air velocity. These data [pints are visualized i figure 5.4, where dark blue area indicates no data, yellow area indicates the applicable region while the light blue area indicates the area

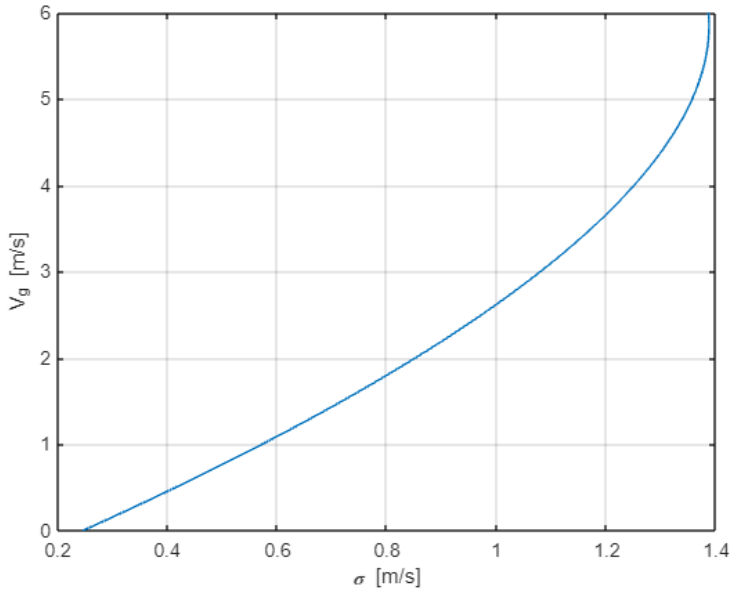

Figure 5.3: V vs σ

where the approximation is not applicable.

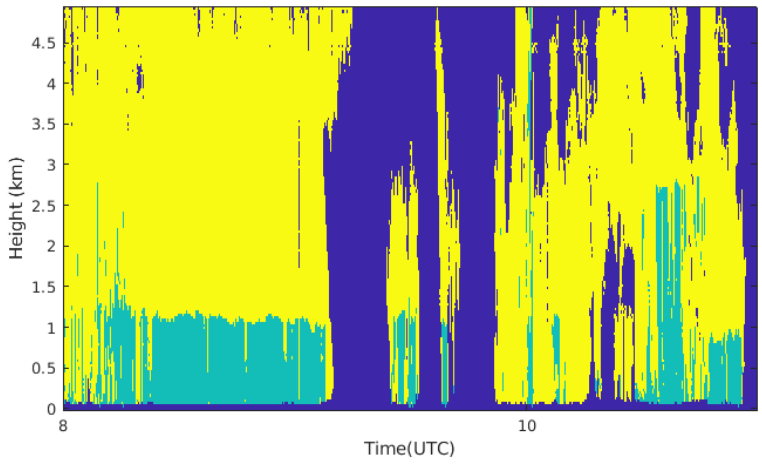

Figure 5.4: Datapoints in an example data file that lie within the σ bounds, indicating the applicability of the 4th order polynomial approximation

In order to address this problem, a relation between fall velocity and the spectrum width with larger fall velocities is investigated. It revealed that when a similar curve is plotted with the terminal velocities now extended to 9m/s as opposed to the previous 6m/s the curve of such a relationship peaks at a spectrum width of 1.4m/s and a velocity of 6.01m/s. This can be observed in figure 5.5.

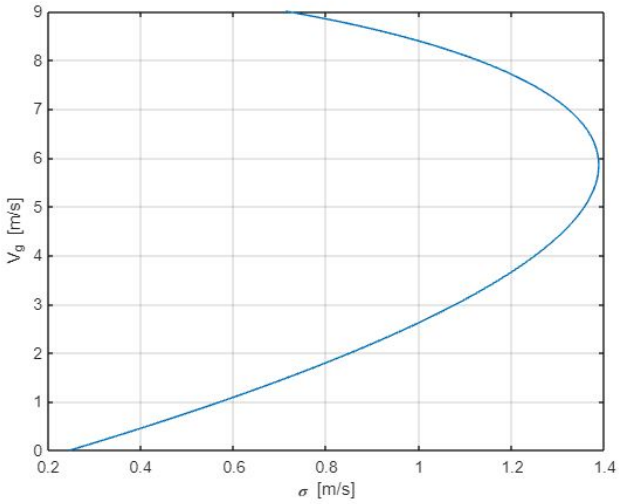

Figure 5.5: V vs σ for V=0-9m/s

Therefore a limiting spectrum width of 1.4m/s is now considered, and based on this curve, as shown in figure 5.6, a new fifth-order polynomial approximation is proposed. As opposed to the previously proposed approximation this is a closer fit as shown in 5.11. By introducing this the applicability is improved. In a section of the data file with continuous precipitation, it is enhanced. A significant improvement in the applicability is seen when only the region of precipitation is considered. An improvement of 34% is seen.

$$\langle v \rangle (\sigma) = \begin{cases} 25.3162\sigma^5 - 96.07577\sigma^4 + 139.2092\sigma^3 - 94.1875\sigma^2 + 32.5521\sigma - 4.1618 & \text{for } \sigma < 1.2761 \\ 6.0144 & \text{for } \sigma \geq 1.2761 \end{cases} \tag{5.11}$$

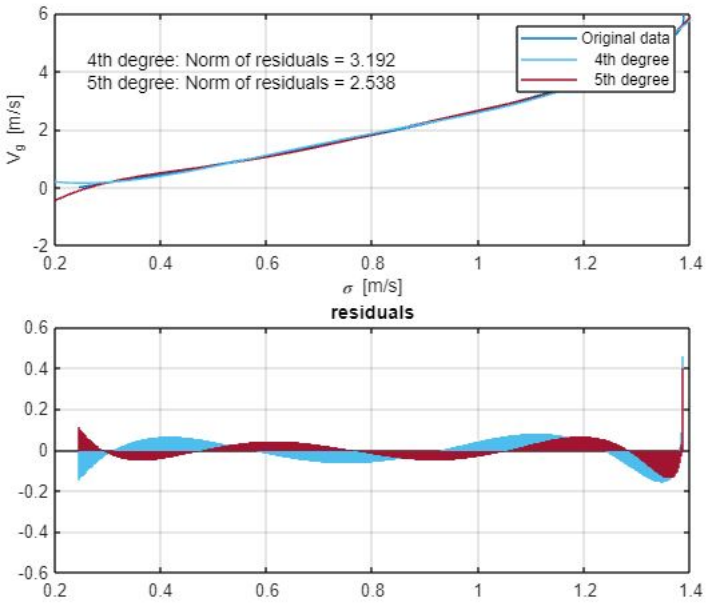

Figure 5.6: Vg vs σ

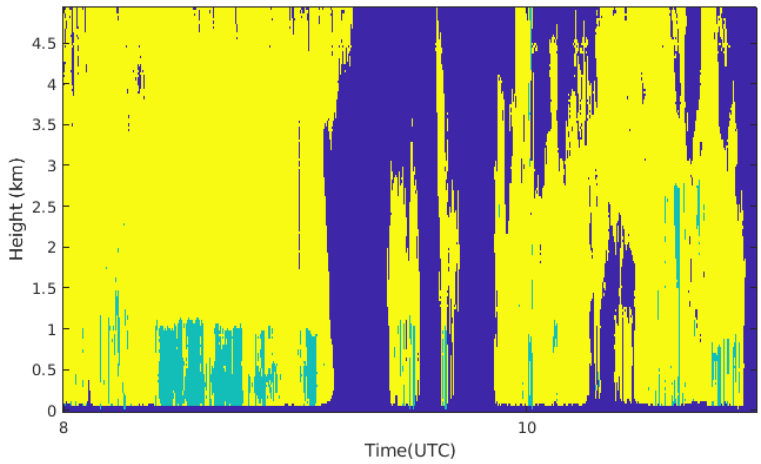

Figure 5.7: Datapoints in an example data file that lie within new σ bounds, indicating the increased applicability of the 5th order polynomial approximation

The next step is to derive the parameters of the drop size distribution to further investigate the physical implications of the proposed algorithm. The parameters of drop size distribution can be derived as follows.

The variable N_0 derived from the expression of reflectivity as shown in equation 5.12 and the mean diameter D_0 which is the inverse of the slope parameter λ is calculated from the terminal velocity as shown in 5.13.

$$N_0 = \frac{Z\Lambda^7}{\Gamma(7)} \tag{5.12}$$

$$\Lambda = \frac{\beta}{\left[\frac{1}{\alpha}\left(1 - \frac{V_{Term}}{V_0}\right)\right]^{-1/7} - 1} \tag{5.13}$$

where $\alpha = 1.07, \beta = 600m^{-1}, V_0 = 9.65m/s$

Forward Model: In order to further investigate the relation between fall velocity and spectrum width, a forward model considering the Marshall-Palmer drop size distribution is created and all the parameters- The reflectivity (Z), mean Doppler velocity(v), and the Doppler spectrum width (σ) as per equations 5.4, 5.5, 5.6 respectively are simulated. The variation of the reflectivity and the velocity with respect to the drop diameter D is given in figure 5.8. The simulated Doppler spectra for different D_0 values are shown in figure 5.9.

The relationship between different mean diameters D_0 and the spectrum width is also explored σ. The widest spectrum width can be found at $D_0 = 1.2m/s$. Beyond this, the width is observed to drop for all subsequent values of $D0$. Thus there is a need to explore the causes behind the broadening of the the spectrum.

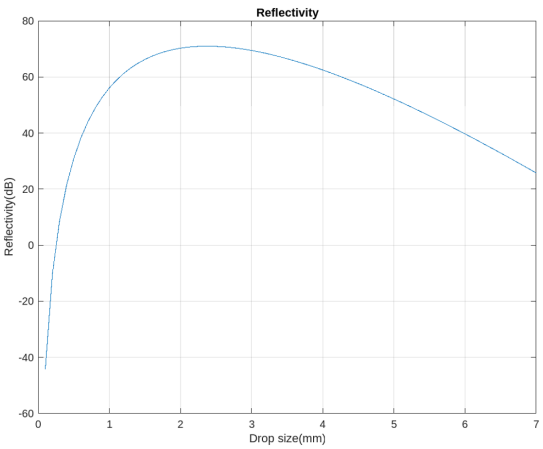

(a) Variation of reflectivity with drop size

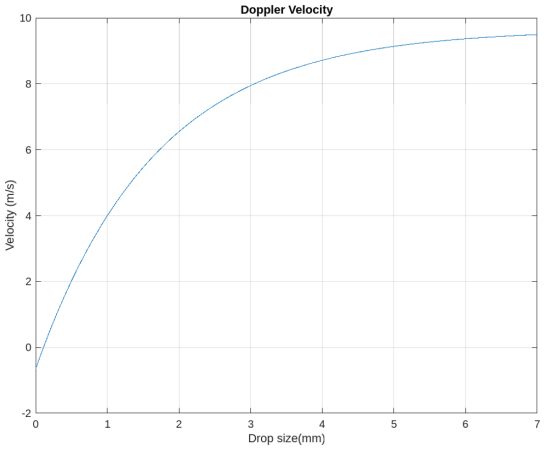

(b) Variation of terminal velocity with drop size

Figure 5.8: Simulated radar measurables

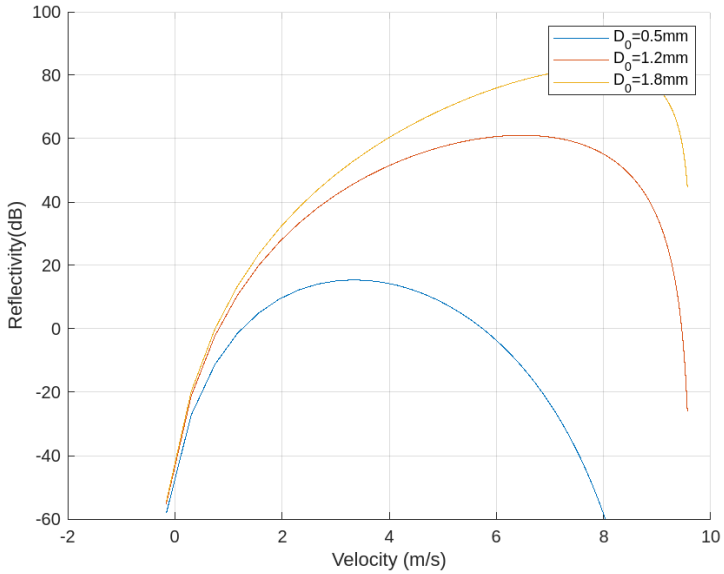

Figure 5.9: Simulated Doppler spectra

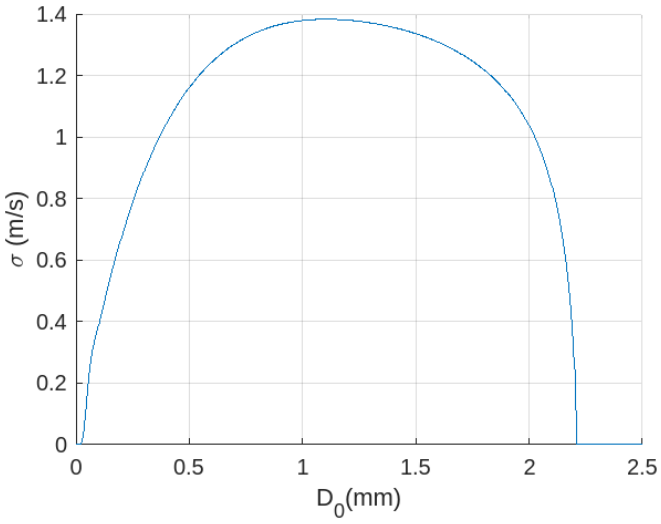

Figure 5.10: Relation between σ and D_0

Investigating spectral broadening: Several factors affect the broadening of the spectral width. It is a function of radar system parameters like beamwidth, signal processing schemes, and so on, as well as meteorological data like the distribution of hydrometeors and velocity within the resolution volume [38]. Some of these factors are as follows. The non-uniform raindrops in the radar beam cause changes in the Doppler shifts of the scattered signals, leading to the spectrum's broadening. Turbulence has a similar effect where the turbulent motion of the air molecules introduces fluctuations in the Doppler shifts leading to the broadening of the spectrum. As distance from the radar increases, the raindrops become increasingly unevenly distributed with fluctuations coupled with the radial wind motions causing further broadening [38]. Errors introduced due to the system's limitations such as temporal and frequency resolution, as well as the impact of noise and calibration errors might lead to further broadening. Considering all these factors, and the analysis of the data, it is fair to say that the limit of the spectral width (1.4m/s) for the applicability of the polynomial approximation is reasonable and wider spectrum widths may be attributed to any of the above-mentioned factors.

5.3. Statistics

The distributions of the variables were studied using histograms. Studying the distribution of variables is an important part of understanding and analyzing data along with laying the foundation for different retrieval techniques. The results showed that the distribution of the spectrum width is distributed as a sum of two gamma functions as can be observed in figure 5.11.

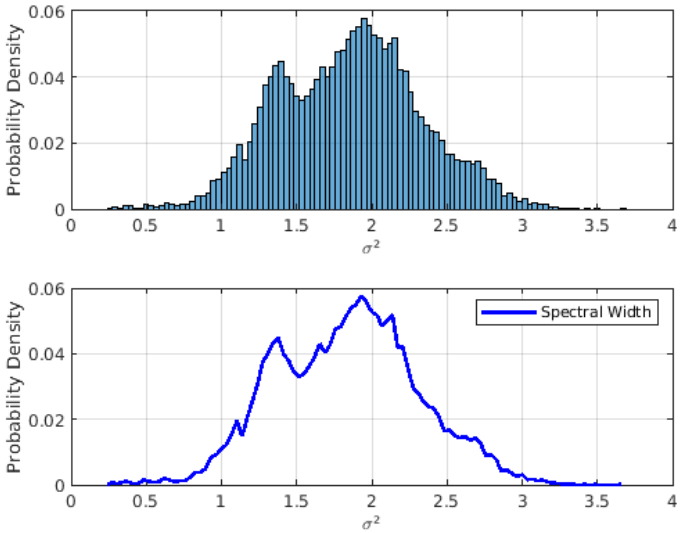

Figure 5.11: Distribution of σ^2 (24-05-21 (0200-0800UTC))

While the vertical air velocity is distributed normally. The few data points that fall outside of the normal distribution are likely to be outliers. This normal distribution may be attributed to the random nature of air motion as well as the balance between updrafts and downdrafts. However, it is important to note that it behaves slightly differently in the regions of precipitation, clouds, and the melting layer. For the observed data file, in the precipitation region, the distribution is shifted to -1m/s indicating a moderate updraft. Within the cloud region, the velocities remain very small and do not exceed 1/ms. Within the melting layer, the air motion is slightly more turbulent, and air has velocities centred around 0.8m/s indicating a weak downdraft.

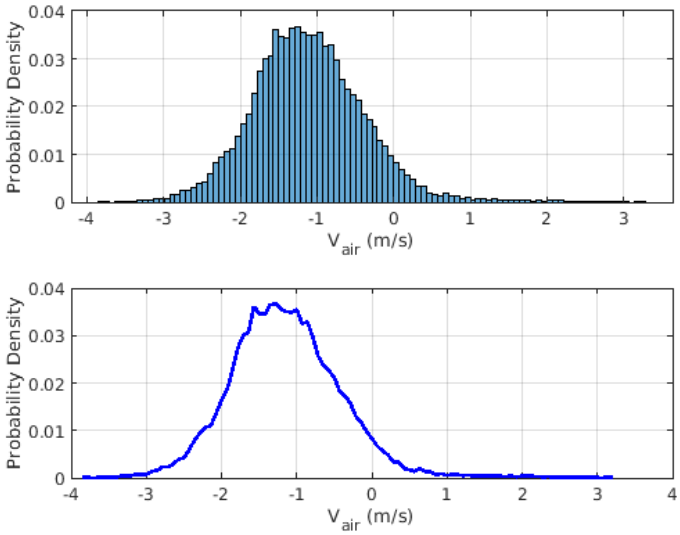

Figure 5.12: Distribution of V_{air} in rain region (24-05-21 (0200-0800UTC))

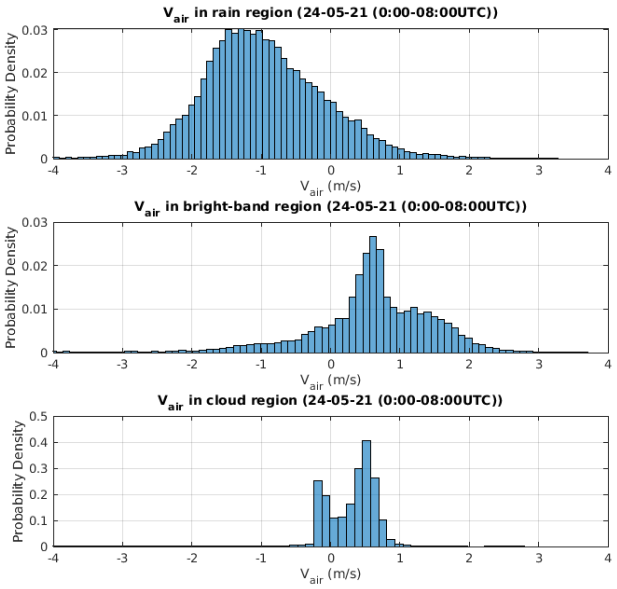

Figure 5.13: Distribution of V_{air} in all three regions (24-05-21 (0200-0800UTC))

This can also be seen in figure 5.14 which represents the occurrence of different velocities at various altitudes, the above-mentioned biases can be observed in this figure as well, for all three regions. In this figure, the black line represents the mean velocity, and the red lines represent the velocity one standard deviation apart.

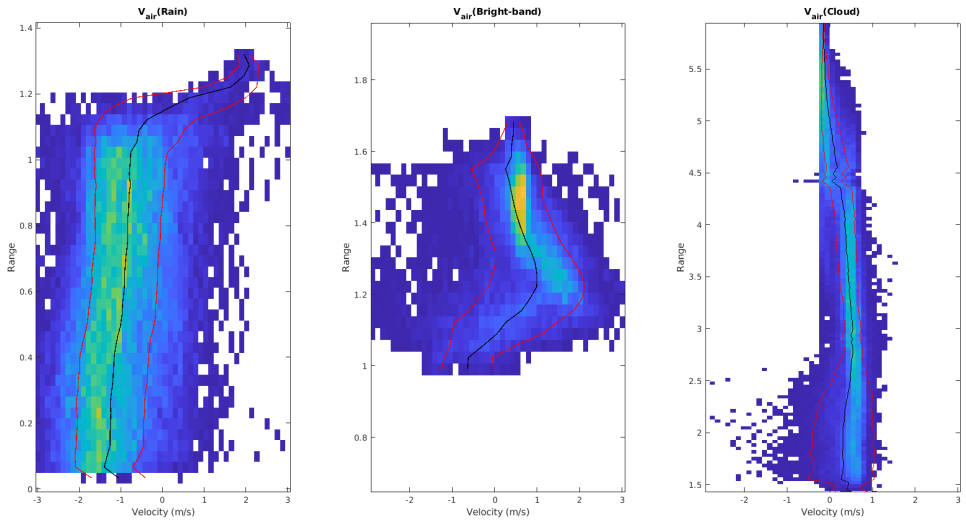

Figure 5.14: Occurrence of velocities at different altitudes

5.4. Criteria for Quality of Retrievals

The absence of true values of the vertical air velocities gives rise to the need to develop several criteria to gauge the quality of retrievals and consequently analyze and validate the performance of the proposed algorithm

Data spikes outliers: The first criterion considered is the presence of data spikes and outliers. This is done by using a median filter. A median filter is a digital signal processing technique that is widely used to smooth or reduce noise in pictures or time series data. It replaces each data point with the median value within a set window or neighbourhood surrounding that point. This is done by moving a window through the data. Within this window, the median value is calculated. This calculated median replaces the original data point at the centre of the window. This process is repeated as the window is shifted to cover each data point, effectively smoothing the data [39]. The objective of using it is to obtain a smoothed form of the data and identify data spikes and outliers by comparing it to the original vertical air velocity data. This calculation provides insights into the extent of deviations from the smoothed data and identifies outliers or irregularities. The identification of these outliers is done based on a spike threshold. This threshold is decided by analyzing the difference between the smoothed data and the original data. The threshold is set to 2m/s.

Temporal consistency The second criterion is to check the temporal consistency of the retrieved velocities. In reality, consecutive measurements need to have a certain level of temporal stability and coherence. Hence it is possible to identify erroneous retrievals by verifying the temporal continuity. This is done by considering the difference between consecutive measurements across the data and setting a threshold. This threshold is set by considering the mean and standard deviation observed in the differences. In this case, the threshold is set at 1.5m/s.

Physical consistency The third criterion is to check the consistency of the air velocities with some of the physical constraints. This is an extension of the first two criteria to ensure that the maximum air velocity is limited and erroneous values that are extremely high are not included. These three criteria are imposed on the data set to verify the performance of the algorithm thus checking the quality of the retrievals.

5.5. Results

The developed algorithm is now applied to the available data, and results are presented in this section. Initially, the applicability of the algorithm is checked for each data file, and the monthly averaged percentage of data points where the algorithm is applicable is shown in table 5.1. It is evident from this applicability study that the proposed algorithm can be effectively utilised across all the months. Despite the spectral broadening introduced by a number of factors as discussed in the previous section, the spectrum width is largely confined to 1.4m/s.

Month	Applicability (%)
January 2021	98
February 2021	95
March 2021	97

Month	Applicability (%)
April 2021	99
May 2021	96
June 2021	95

Table 5.1: Applicability of algorithm across six months

The algorithm is applied to the dataset, the vertical profile of the retrieved air velocity and the measured mean Doppler velocity are presented in figure 5.15, and the time average profile for the same is shown in figure 5.16. Following this, the vertical profiles of mean drop diameter D_0 is given in figure 5.17.

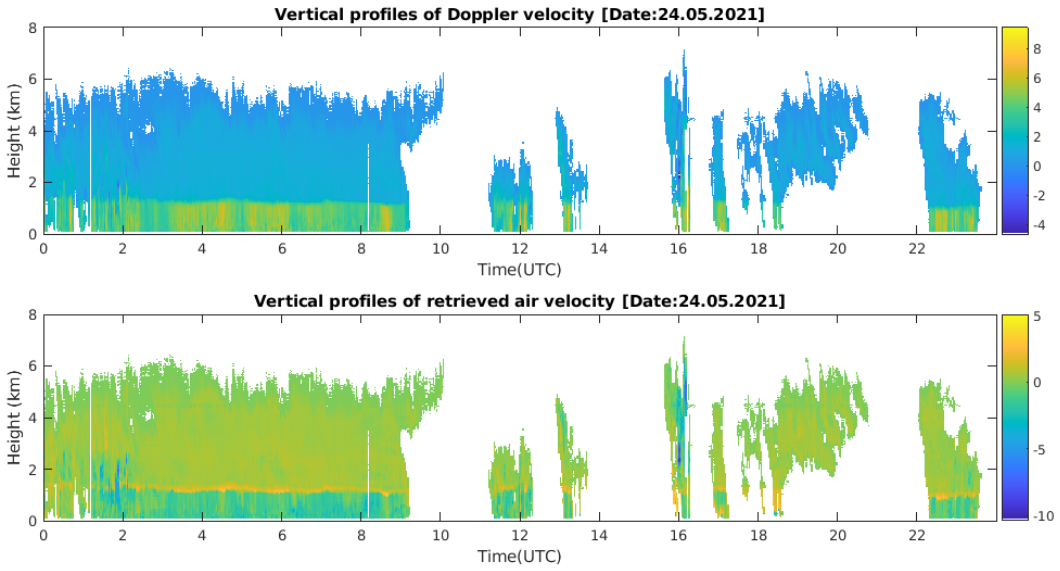

Figure 5.15: Vertical profiles of mean Doppler velocity and the retrieved vertical air velocity

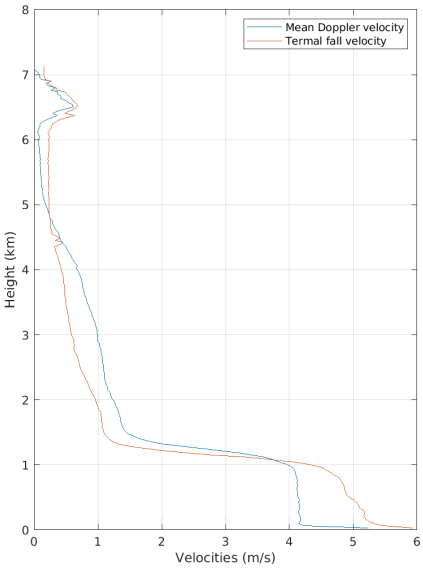

(a) Retrieved terminal velocity of rain drops and mean Doppler velocity

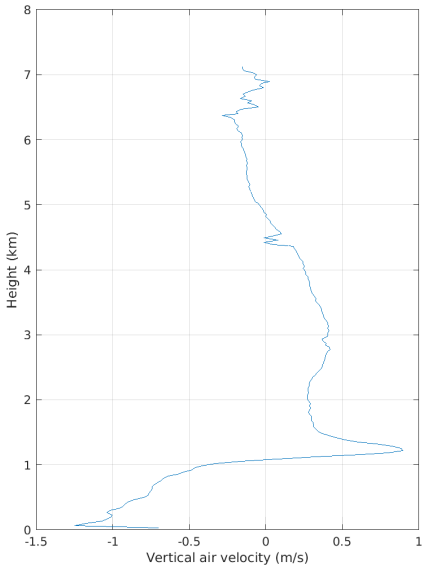

(b) Retrieved vertical air velocity

Figure 5.16: Retrievals by using the proposed σ-V relation

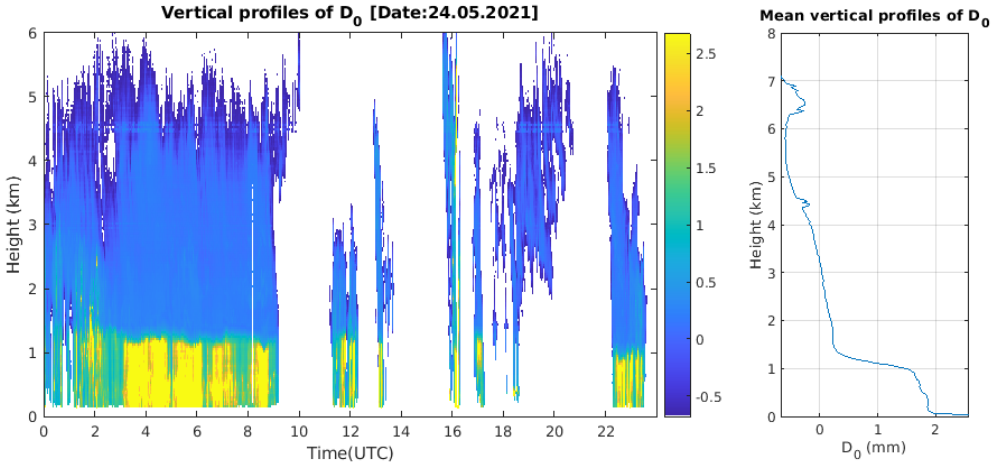

Figure 5.17: Vertical profiles of D_0

Quality control criteria By imposing the quality control criteria across the data of six months it was found that the retrieval algorithm performs satisfactorily. The percentages of data points flagged as erroneous for each month are shown in table 5.2. As can be seen from the table, a slightly higher percentage is observed in the month of May, this may be a result of heavy turbulent precipitation events, wherein there is high variability in the consecutive air velocities. This may be indicative that the true value might be lower. However, in order to ensure the identification of erroneous velocities in other months, the thresholds can not be modified. The flagged datapoints are visualized in red as shown in figure **??**

Month	Data points flagged (%)
January 2021	0.96

Month	Data points flagged (%)
February 2021	0.45
March 2021	0.64
April 2021	1.26
May 2021	1.70
June 2021	1.36

Table 5.2: Percentage of data points flagged as erroneous across six months

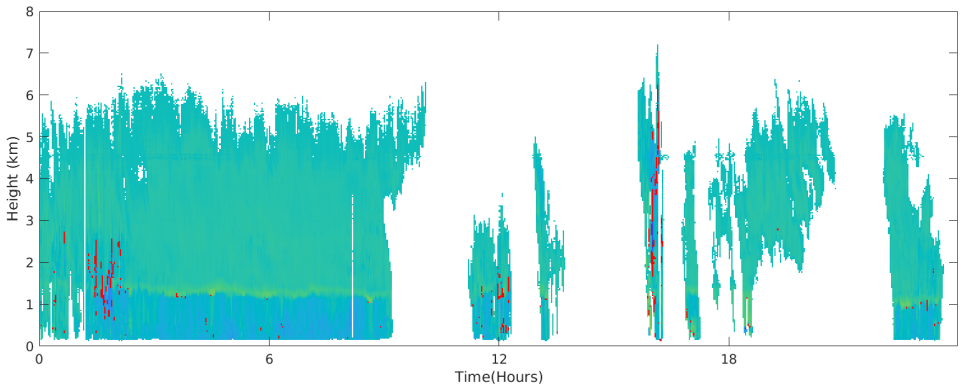

Figure 5.18: Visualization of erroneous data points

5.6. Conclusion

This section detailed the algorithm used to calculate vertical air velocity. Following a study of the literature, the suggested algorithm is addressed, the criteria for the quality of the retrievals are explained, and finally, the results are provided. By analysing the statistics of the data, multiple insights can be drawn regarding the distribution of velocities and the occurrence of these velocities at different altitudes.

6

Conclusion

6.1. Conclusions

In conclusion, this thesis has presented a comprehensive investigation into the retrieval of vertical air velocities, various data processing techniques to enhance data quality and reliability as well as a rain type and hydrometeor classification schemes. The findings obtained from the extensive analysis and experimentation have provided insights into the various atmospheric processes that govern and affect vertical air motions and the study of which can aid in better understanding the complex nature of the retrieval problem. Throughout this research, the primary objectives have been to develop algorithms for the retrieval of vertical air velocity, which involves relating various parameters of the drop size distribution to radar measurements. The second objective was to carry out the classification of precipitation types and hydrometeor classes. The next was to develop retrieval quality criteria and analyze the accuracy of the results obtained from the proposed algorithm. Lastly, the research also aimed to develop an algorithm for optimal data processing, and "big data"-based analysis of retrieval techniques for validating the performance of all the aforementioned algorithms. These objectives served as the guiding framework for the entire study.

Despite the advancements in radar technology, the accurate retrieval of air velocities remains a challenge due to a number of reasons including the need for reliable and high-quality radar data, variations in the vertical reflectivity profiles and the errors induced in the estimation of the drop size parameters. This thesis proposes multiple strategies to mitigate the impact of these challenges. Firstly, a comprehensive data processing pipeline has been implemented which transforms raw radar data into reliable high-quality data by undertaking a number of techniques. The first step involves the removal of noise and clutter from the data. This is done by creating a target mask to isolate the desired meteorological targets (precipitation, clouds and so on) from the various forms of clutter and noise introduced due to biological targets, clear sky reflections, and other non-meteorological or erroneous echoes. This target mask is created by imposing thresholds on the reflectivity and Doppler spectrum width based on

the typical values for meteorological targets, by exploiting the polarimetric features of differential reflectivity and linear depolarization ratio, and lastly by using morphological filtration technique to remove speckle noise from the data. All parameters have been optimized by utilizing a number of data files with diverse rainfall types and clutter characteristics. The sparsity of data segments is analysed unsuitable segments are discarded. It is observed high levels of sparsity are observed at altitudes greater than 6km. To make the data processing efficient, the spatial and temporal averaging of the data is carried out, which degrades both the resolutions but still gives sufficiently detailed data for further analyses. Considering the importance of data quality in the thesis, a final quality control criterion based on the correlation between the co-polarized channels is considered. As the measurements are made in the zenith direction the meteorological echoes are expected to show high levels of correlation. It is observed that low altitudes (<100m) show poor correlation and are hence discarded. At this step of the pipeline, the radar data is reliable and suitable to be used for further analysis.

A classification scheme is implemented to differentiate between two rainfall types stratiform and convective. Consequently, the algorithm involves classifying the classes of hydrometeors in the vertical profile of the atmosphere that are characterized by the presence of specific types of hydrometeors present in these said regions. The classification algorithm implemented utilizes the presence of a bright band to classify the rainfall types and bright band detection is done by utilizing the reflectivity, Doppler velocity and Doppler width. The algorithm is able to successfully classify stratiform and convective rainfall events, as well as the classes in the vertical profile. By adopting this classification framework, a robust foundation for accurate rainfall classification is established which contributes to a more comprehensive understanding of precipitation dynamics. Another aspect examined here is the occurrence of the aforementioned classes at different altitudes to develop a better understanding of the trends in the rainfall heights. It is observed that the melting layer occurrence rises to higher altitudes from January to June.

For the retrieval of the air velocities, an algorithm is proposed which relates the Doppler spectrum width to the terminal fall velocity of the raindrops. The applicability of this algorithm is investigated. This is tested for the 6 months of data and it is found that it is applicable in 96.66% cases. A quality criteria is proposed that aims to analyse physical consistencies in the results by comparing the retrievals with physical constraints, temporal and spatial variability of the retrieved air velocity by examining it as a function of altitude and time (over a range of several hours or more) to see trends and remove anomalies. Using this criteria, it is found that an average of 1.06% data points were flagged by this criteria, giving the results a 98.9% success rate. The analysis of distributions of the spectral width, and the retrieved air velocities for the different classes of hydrometeors revealed the Gaussian nature of the air velocity.

To summarize the contributions made by this research, an algorithm for the classification of rainfall types and classes of hydrometeors in the vertical profiles has been developed. Another aspect of this project is to utilize massive data for statistical and performance analysis of velocity retrieval algorithms under various weather conditions over large periods of time, and finally, criteria for the quality of the air-motion retrievals are developed which coupled with the large-scale data analysis quantify the performance of the aforementioned retrieval algorithm. These contributions allow the effective analysis of

the intricate dynamics of the vertical air motions within the atmosphere and provide a comprehensive understanding of the vertical velocity patterns, contributing to meteorological insights and facilitating further advancements in atmospheric research and prediction capabilities.

References

[1] M. S. Binetti, C. Campanale, C. Massarelli, and V. F. Uricchio, "The use of weather radar data: Possibilities, challenges and advanced applications," *Earth 2022, Vol. 3*, vol. 3, pp. 157–171, 1 Feb. 2022. DOI: 10.3390/EARTH3010012.

[2] N. Nanding and M. A. Rico-Ramirez, "Precipitation measurement with weather radars," *Handbook of Environmental Chemistry*, vol. 102, pp. 235–258, 2021. DOI: 10.1007/698_2019_404.

[3] E. Saltikoff, K. Friedrich, J. Soderholm, *et al.*, "An overview of using weather radar for climatological studies: Successes, challenges, and potential," *Bulletin of the American Meteorological Society*, vol. 100, pp. 1739–1752, 9 Sep. 2019. DOI: 10.1175/BAMS-D-18-0166.1.

[4] J. A. Smith, D. J. Seo, M. L. Baeck, and M. D. Hudlow, "An intercomparison study of NEXRAD precipitation estimates," *Water Resources Research*, vol. 32, pp. 2035–2045, 7 Jul. 1996, ISSN: 1944-7973. DOI: 10.1029/96WR00270.

[5] J. Joss, A. Waldvogel, and C. G. Collier, "Precipitation measurement and hydrology," *Radar in Meteorology*, pp. 577–606, 1990. DOI: 10.1007/978-1-935704-15-7_39.

[6] C. Wolff. "Frequency-modulated continuous-wave radar (FMCW radar)." Accessed: 2021-12-06. (), [Online]. Available: https://www.radartutorial.eu/02.basics/Frequency\%20Modulated\%20\\Continuous\%20Wave\%20Radar.en.html.

[7] A. Stove, "Linear FMCW radar techniques," *Proceedings of the IEEE*, 1992.

[8] G. Brooker, "Understanding millimetre wave FMCW radars," *1st International Conference on Sensing Technology*, Jan. 2005.

[9] U. Kumbul, N. Petrov, F. van der Zwan, C. S. Vaucher, and A. Yarovoy, "Experimental investigation of phase coded FMCW for sensing and communications," in *2021 15th European Conference on Antennas and Propagation (EuCAP)*, 2021, pp. 1–5. DOI: 10.23919/EuCAP51087.2021.9411464.

[10] M. A. M. A. Richards, *Fundamentals of radar signal processing*. McGraw-Hill, 2005, p. 513, ISBN: 9780071444743.

[11] Kusmadi and A. Munir, "Performance analysis of FMCW-based X-band weather radar," in *2016 2nd International Conference on Wireless and Telematics (ICWT)*, 2016, pp. 40–43. DOI: 10.1109/ICWT.2016.7870848.

[12] V. N. Bringi and V. Chandrasekar, *Polarimetric Doppler Weather Radar: Principles and applications*. Cambridge University Press, 2005.

[13] G. Lee, V. Bringi, and M. Thurai, "The retrieval of drop size distribution parameters using a dual-polarimetric radar," *Remote Sensing*, vol. 15, no. 4, 2023, ISSN: 2072-4292. DOI: 10.3390/rs15041063. [Online]. Available: https://www.mdpi.com/2072-4292/15/4/1063.

[14] D. Atlas, R. C. Srivastava, and R. S. Sekhon, "Doppler radar characteristics of precipitation at vertical incidence," *Reviews of Geophysics*, vol. 11, pp. 1–35, 1 Feb. 1973, ISSN: 1944-9208. DOI: 10.1029/RG011I001P00001. [Online]. Available: https://onlinelibrary.wiley.com/doi/full/10.1029/RG011i001p00001https://onlinelibrary.wiley.com/doi/abs/10.1029/RG011i001p00001https://agupubs.onlinelibrary.wiley.com/doi/10.1029/RG011i001p00001.

[15] O. A. Krasnov, L. P. Ligthart, Z. Li, G. Babur, Z. Wang, and F. van der Zwan, "PARSAX: High-resolution Doppler-polarimetric FMCW radar with dual-orthogonal signals," in *18-th INTERNATIONAL CONFERENCE ON MICROWAVES, RADAR AND WIRELESS COMMUNICATIONS*, 2010, pp. 1–5.

[16] U. N. U. Guide, *NetCDF users guide: The components of a NetCDF data set*. [Online]. Available: https://docs.unidata.ucar.edu/nug/current/netcdf_data_set_components.html.

[17] D. Giuli, M. Gherardelli, A. Freni, T. A. Seliga, and K. Aydin, "Rainfall and clutter discrimination by means of dual-linear polarization radar measurements," *Journal of Atmospheric and Oceanic Technology*, vol. 8, pp. 777–789, 6 Dec. 1991, ISSN: 15200426. DOI: 10.1175/1520-0426(1991)008.

[18] R. J. Doviak, D. S. Zrnic, and D. S. Sirmans, "Doppler weather radar," *Proceedings of the IEEE*, vol. 67, 1979. DOI: 10.1109/PROC.1979.11511.

[19] H. Leijnse, H. Beekhuis, and I. Holleman, *Doppler clutter removal on KNMI weather radars*, '2016'. [Online]. Available: https://cdn.knmi.nl/knmi/pdf/bibliotheek/knmipubTR/TR355.pdf.

[20] M. Fang and R. Doviak, *Spectrum width statistics of various weather phenomena*, Sep. 2001. [Online]. Available: https://www.nssl.noaa.gov/publications/wsr88d_reports/.

[21] F. Silvestro, N. Rebora, L. Ferraris, M. Morando, P. Alberoni, and A. Fornasiero, "Clutter and rainfall discrimination by means of doppler-polarimetric measurements and vertical reflectivity profile analysis," *Advances in Geosciences*, vol. 2, pp. 135–138, 2005, ISSN: 16807359. DOI: 10.5194/ADGEO-2-135-2005. [Online]. Available: https://www.researchgate.net/publication/26438250_Clutter_and_rainfall_discrimination_by_means_of_doppler-polarimetric_measurements_and_vertical_reflectivity_profile_analysis.

[22] C. Sandford, A. Illingworth, and R. Thompson, "The potential use of the linear depolarization ratio to distinguish between convective and stratiform rainfall to improve radar rain-rate estimates," *Journal of Applied Meteorology and Climatology*, vol. 56, pp. 2927–2940, 11 Nov. 2017, ISSN: 1558-8424. DOI: 10.1175/JAMC-D-17-0014.1. [Online]. Available: https://journals.ametsoc.org/view/journals/apme/56/11/jamc-d-17-0014.1.xml.

[23] T. A. Seliga and V. N. Bringi, "Potential use of radar differential reflectivity measurements at orthogonal polarizations for measuring precipitation," *Journal of Applied Meteorology and Climatology*, vol. 15, no. 1, pp. 69 –76, 1976. DOI: https://doi.org/10.1175/1520-0450(1976)015<0069:PUORDR>2.0.CO;2. [Online]. Available: https://journals.ametsoc.org/view/journals/apme/15/1/1520-0450_1976_015_0069_puordr_2_0_co_2.xml.

[24] C. Unal, "Spectral polarimetric radar clutter suppression to enhance atmospheric echoes," *Journal of Atmospheric and Oceanic Technology*, vol. 26, no. 9, pp. 1781 –1797, 2009. DOI: https://doi.org/10.1175/2009JTECHA1170.1. [Online]. Available: https://journals.ametsoc.org/view/journals/atot/26/9/2009jtecha1170_1.xml.

[25] P. Maragos and R. Schafer, "Morphological systems for multidimensional signal processing," *Proceedings of the IEEE*, vol. 78, no. 4, pp. 690–710, 1990. DOI: 10.1109/5.54808.

[26] W. Ghada, E. Casellas, J. Herbinger, *et al.*, "Stratiform and convective rain classification using machine learning models and micro rain radar," *Remote Sensing 2022, Vol. 14, Page 4563*, vol. 14, p. 4563, 18 Sep. 2022, ISSN: 2072-4292. DOI: 10.3390/RS14184563. [Online]. Available: https://www.mdpi.com/2072-4292/14/18/4563/htmhttps://www.mdpi.com/2072-4292/14/18/4563.

[27] C. R. Williams, W. L. Ecklund, and K. S. Gage, "Classification of precipitating clouds in the tropics using 915-MHz wind profilers," *Journal of Atmospheric and Oceanic Technology*, vol. 12, pp. 996–1012, 1995.

[28] A. B. White, P. J. Neiman, F. M. Ralph, D. E. Kingsmill, and P. O. G. Persson, "Coastal orographic rainfall processes observed by radar during the california land-falling jets experiment," *Journal of Hydrometeorology*, vol. 4, no. 2, pp. 264 –282, 2003. DOI: https://doi.org/10.1175/1525-7541(2003)4<264:CORPOB>2.0.CO;2. [Online]. Available: https://journals.ametsoc.org/view/journals/hydr/4/2/1525-7541_2003_4_264_corpob_2_0_co_2.xml.

[29] M. Thurai, P. Gatlin, and V. Bringi, "Separating stratiform and convective rain types based on the drop size distribution characteristics using 2d video disdrometer data," *Atmospheric Research*, vol. 169, Apr. 2015. DOI: 10.1016/j.atmosres.2015.04.011.

[30] N. Gil-de Vergara, J. Riera, S. Pérez-Peña, J. Garcia-Rubia, and A. Benarroch, "Classification of rainfall events and evaluation of drop size distributions using a k-band doppler radar," Jan. 2018, 829 (5 pp.)–829 (5 pp.) DOI: 10.1049/cp.2018.1188.

[31] M. A. Rico-Ramirez and I. D. Cluckie, "Bright-band detection from radar vertical reflectivity profiles," *International Journal of Remote Sensing*, vol. 28, pp. 4013–4025, 18 Sep. 2007, ISSN: 13665901. DOI: 10.1080/01431160601047797. [Online]. Available: https://www.researchgate.net/publication/261990678_Bright_Band_detection_from_radar_vertical_reflectivity_profiles.

[32] J. S. Marshall and W. M. K. Palmer, "The distribution of raindrops with size," *Journal of the Atmospheric Sciences*, vol. 5, pp. 165–166, 4 Aug. 1948. DOI: 10.1175/1520-0469(1948)005. [Online]. Available: https://journals.ametsoc.org/view/journals/atsc/5/4/1520-0469_1948_005_0165_tdorws_2_0_co_2.xml.

[33] A. Waldvogel, "The n0 jump of raindrop spectra," *Journal of Atmospheric Sciences*, vol. 31, no. 4, pp. 1067 –1078, 1974. DOI: https://doi.org/10.1175/1520-0469(1974)031<1067:TJORS>2.0.CO;2. [Online]. Available: https://journals.ametsoc.org/view/journals/atsc/31/4/1520-0469_1974_031_1067_tjors_2_0_co_2.xml.

[34] C. W. Ulbrich, "Natural variations in the analytical form of the raindrop size distribution," *Journal of Applied Meteorology and Climatology*, vol. 22, no. 10, pp. 1764 –1775, 1983. DOI: https://doi.org/10.1175/1520-0450(1983)022<1764:NVITAF>2.0.CO;2. [Online]. Available: https://journals.ametsoc.org/view/journals/apme/22/10/1520-0450_1983_022_1764_nvitaf_2_0_co_2.xml.

[35] Q. Cao, G. Zhang, E. Brandes, T. Schuur, A. Ryzhkov, and K. Ikeda, "Analysis of video disdrometer and polarimetric radar data to characterize rain microphysics in oklahoma," *Journal of Applied Meteorology and Climatology*, vol. 47, no. 8, pp. 2238 –2255, 2008. DOI: https://doi.org/10.1175/2008JAMC1732.1. [Online]. Available: https://journals.ametsoc.org/view/journals/apme/47/8/2008jamc1732.1.xml.

[36] M. Pinsky, Private communication, 2023.

[37] M. Pinsky, O. A. Krasnov, A. Khain, and P. Khain, "The turbulence structure of isolated Cu as derived from high resolution vertically pointing Doppler radar," *submitted to Journal Atmospheric Sciences*, Aug. 2023.

[38] R. J. Doviak and D. S. Zrnić, "5 - doppler spectra of weather signals," in *Doppler Radar and Weather Observations (Second Edition)*, R. J. Doviak and D. S. Zrnić, Eds., Second Edition, San Diego: Academic Press, 1993, pp. 87–121, ISBN: 978-0-12-221422-6. DOI: https://doi.org/10.1016/B978-0-12-221422-6.50010-3. [Online]. Available: https://www.sciencedirect.com/science/article/pii/B9780122214226500103.

[39] S. Villar, S. Torcida, and G. Acosta, "Median filtering: A new insight," *Journal of Mathematical Imaging and Vision*, vol. 58, pp. 1–17, May 2017. DOI: 10.1007/s10851-016-0694-0.

A

Contents of NetCDF File

Variable Name	Dimensions	Attributes
latitude	zero	Latitude of radar position [degrees_north]
longitude	zero	Longitude of radar position [degrees_east]
altitude	zero	Altitude of antenna above sea level [m]
current_day	zero	Julian Day/Time [julian day/time]
number_of_campaigns	zero	Number of Measurement Campaigns in current daily file
Attenuation_mode	campaign	Type of attenuation control
Current_Campaign	campaign	Current Campaign Type
Antenna_Mode	campaign	Current antenna mode
FFT_Windows Proc_Dop	campaign	Window Type for Doppler Processing
Proc_FPGA_Algoritm	campaign	FPGA Algorithm
Radar_Frequency	campaign	Radar Frequency [GHz]
Sampling_Part	campaign	Sampling part of FPGA [fractional]
WF_H_Tr	campaign	Waveform, transmitted via H-channel
WF_V_Tr	campaign	Waveform, transmitted via V-channel
WF_H_Ref	campaign	Waveform, reference via H-channel
WF_V_Ref	campaign	Waveform, reference via V-channel
WF_H_Tr_Bandwidth	campaign	Bandwidth of transmitted via H-channel waveform [MHz]
WF_V_Tr_Bandwidth	campaign	Bandwidth of transmitted via V-channel waveform [MHz]
WF_H_Ref_Bandwidth	campaign	Bandwidth of reference via H-channel waveform [MHz]
WF_V_Ref_Bandwidth	campaign	Bandwidth of reference via V-channel waveform [MHz]
Sweep_Time	campaign	Sweep time [ms]
campaign_number	time	Number of Current Measurement Campaign

Variable Name	Dimensions	Attributes
attenuation_H	time	Attenuation in H-channel [dB]
attenuation_V	time	Attenuation in V-channel [dB]
amplifier_level_H	time	Amplifier level in H-channel [dBm]
amplifier_level_V	time	Amplifier level in V-channel [dBm]
Analog_TX_H	time	Analog transmitter power horizontal [dBm]
Analog_TX_V	time	Analog transmitter power vertical [dBm]
Analog_RX_H	time	Analog received power horizontal [dBm]
Analog_RX_V	time	Analog received power vertical [dBm]
reflectivity_HH	range , time	Radar reflectivity factor [dBz]
velocity_HH	range , time	Velocity [m/s]
width_HH	range , time	Spectral width [m/s]
reflectivity_HV	range , time	Radar reflectivity factor [dBz]
velocity_HV	range , time	Velocity [m/s]
width_HV	range , time	Spectral width [m/s]
reflectivity_VH	range , time	Radar reflectivity factor [dBz]
velocity_VH	range , time	Velocity [m/s]
width_VH	range , time	Spectral width [m/s]
reflectivity_VV	range , time	Radar reflectivity factor [dBz]
velocity_VV	range , time	Velocity [m/s]
width_VV	range , time	Spectral width [m/s]
current_time	time	
antenna_azimuth	time	Antenna Azimuth angle [degree]
antenna_elevation	time	Antenna Elevation angle [degree]
antenna_polarization	time	Orientation of Antenna Polarization Basis [degree]

Table A.1: Contents of NetCDF File